J|A|C|S ARTICLES

Published on Web 03/03/2010

Site-Specific Backbone Amide ^{15}N Chemical Shift Anisotropy Tensors in a Small Protein from Liquid Crystal and Cross-Correlated Relaxation Measurements

Lishan Yao,[†] Alexander Grishaev,[†] Gabriel Cornilescu,[‡] and Ad Bax*,[†]

Laboratory of Chemical Physics, NIDDK, National Institutes of Health, Bethesda, Maryland 20892-0520, and National Magnetic Resonance Facility, Madison, Wisconsin 53706

Received December 2, 2009; E-mail: bax@nih.gov

Abstract: Site-specific ^{15}N chemical shift anisotropy (CSA) tensors have been derived for the well-ordered backbone amide ^{15}N nuclei in the B3 domain of protein G (GB3) from residual chemical shift anisotropy (RCSA) measured in six different mutants that retain the native structure but align differently relative to the static magnetic field when dissolved in a liquid crystalline Pf1 suspension. This information is complemented by measurement of cross-correlated relaxation rates between the ^{15}N CSA tensor and either the ^{15}N$-^{1}$H or ^{15}N$-^{13}$C′ dipolar interaction. In agreement with recent solid state NMR measurements, the ^{15}N CSA tensors exhibit only a moderate degree of variation from averaged values, but have larger magnitudes in α-helical (-173 ± 7 ppm) than in β-sheet (-162 ± 6 ppm) residues, a finding also confirmed by quantum computations. The orientations of the least shielded tensor component cluster tightly around an in-peptide-plane vector that makes an angle of $19.6 \pm 2.5°$ with the N−H bond, with the asymmetry of the ^{15}N CSA tensor being slightly smaller in α-helix ($\eta = 0.23 \pm 0.17$) than in β-sheet ($\eta = 0.31 \pm 0.11$). The residue-specific ^{15}N CSA values are validated by improved agreement between computed and experimental ^{15}N $R_{1\rho}$ relaxation rates measured for ^{15}N-{^{2}H} sites in GB3, which are dominated by the CSA mechanism. Use of residue-specific ^{15}N CSA values also results in more uniform generalized order parameters, S^2, and predicts considerable residue-by-residue variations in the magnetic field strengths where TROSY line narrowing is most effective.

Introduction

Chemical shifts play an increasingly important role in NMR analyses of protein structure and dynamics.[1−6] Although the structural dependence of ^{1}H and ^{13}C chemical shifts is known reasonably well, both on the basis of empirical and computational studies,[7−13] backbone amide ^{15}N chemical shifts are less well understood and many factors have been reported to impact them, including residue type, backbone torsion angles, hydrogen bonding, the intraresidue χ_1 angle, and the side chain of the preceding residue.[14−21] The isotropic ^{15}N shift corresponds to the trace of its anisotropic chemical shielding tensor, and a quantitative analysis of factors impacting the isotropic shift hinges on an understanding of the role each of the structural parameters has on the six independent variables that make up the symmetric part of this tensor.

For solid state NMR applications, valuable structural information is encapsulated in the ^{15}N chemical shielding anisotropy. In particular, when studying oriented peptide or protein samples, the observed chemical shift provides information on the orientation of the peptide group relative to the magnetic field, which becomes a particularly powerful structural restraint when combined with the orientation of the ^{15}N$-^{1}$H bond, contained in its dipolar coupling.[22−24] For solution NMR, interference

[†] National Institutes of Health.
[‡] National Magnetic Resonance Facility.

(1) Berjanskii, M. V.; Wishart, D. S. *J. Am. Chem. Soc.* **2005**, *127*, 14970–14971.
(2) Cavalli, A.; Salvatella, X.; Dobson, C. M.; Vendruscolo, M *Proc. Natl. Acad. Sci. U. S. A.* **2007**, *104*, 9615–9620.
(3) London, R. E.; Wingad, B. D.; Mueller, G. A. *J. Am. Chem. Soc.* **2008**, *130*, 11097–11105.
(4) Vila, J. A.; Aramini, J. M.; Rossi, P.; Kuzin, A.; Su, M.; Seetharaman, J.; Xiao, R.; Tong, L.; Montelione, G. T.; Scheraga, H. A *Proc. Natl. Acad. Sci. U. S. A.* **2008**, *105*, 14389–14394.
(5) Villegas, M. E.; Vila, J. A.; Scheraga, H. A. *J. Biomol. NMR* **2007**, *37*, 137–146.
(6) Shen, Y.; Delaglio, F.; Cornilescu, G.; Bax, A. *J. Biomol. NMR* **2009**, *44*, 213–223.
(7) Saito, H. *Magn. Reson. Chem.* **1986**, *24*, 835–852.
(8) Wishart, D. S.; Sykes, B. D.; Richards, F. M. *J. Mol. Biol.* **1991**, *222*, 311–333.
(9) Case, D. A. *J. Biomol. NMR* **1995**, *6*, 341–346.
(10) Wagner, G.; Pardi, A.; Wuthrich, K. *J. Am. Chem. Soc.* **1983**, *105*, 5948–5949.
(11) Williamson, M. P.; Asakura, T. *J. Magn. Reson. B* **1993**, *101*, 63–71.
(12) Bim, J.; Poon, A.; Mao, Y.; Ramamoorthy, A. *J. Am. Chem. Soc.* **2004**, *126*, 8529–8534.
(13) Birn, J.; Poon, A.; Ramamoorthy, A. *Biophys. J.* **2004**, *86*, 73A–73A.
(14) Le, H. B.; Oldfield, E. *J. Phys. Chem.* **1996**, *100*, 16423–16428.
(15) Brender, J. R.; Taylor, D. M.; Ramamoorthy, A. *J. Am. Chem. Soc.* **2001**, *123*, 914–922.
(16) Wang, Y. J.; Jardetzky, O. *J. Am. Chem. Soc.* **2002**, *124*, 14075–14084.
(17) Xu, X. P.; Case, D. A. *Biopolymers* **2002**, *65*, 408–423.
(18) Wang, Y. J.; Jardetzky, O. *J. Biomol. NMR* **2004**, *28*, 327–340.
(19) Poon, A.; Birn, J.; Ramamoorthy, A. *J. Phys. Chem. B* **2004**, *108*, 16577–16585.
(20) Cai, L.; Fushman, D.; Kosov, D. S. *J. Biomol. NMR* **2008**, *41*, 77–88.
(21) Waddell, K. W.; Chekmenev, E. Y.; Wittebort, R. J. *J. Am. Chem. Soc.* **2005**, *127*, 9030–9035.

between the ^{15}N CSA and $^{15}N-^{1}H$ dipolar relaxation mechanisms forms the basis for the all-important TROSY experiment, which dramatically enhances resolution in protein NMR spectroscopy.[25] Quantitative analysis of ^{15}N relaxation rates, which depends on the ^{15}N CSA tensor, can provide detailed information on internal dynamics of the protein backbone.[26−28] To date, nearly all analysis have been carried out under the assumption of a uniform value for the ^{15}N CSA tensor, often assumed to be axially symmetric with a magnitude, $\Delta\sigma$, of −160 or −170 ppm.[27,29] However, early single crystal solid state NMR measurements by Hiyama et al. on Boc-glycylglycyl[^{15}N]glycine benzyl ester showed large variations in the CSA asymmetry, from nearly axially symmetric in a monoclinic lattice form, to quite asymmetric ($\eta = 0.44$) in a triclinic lattice.[30] Numerous subsequent studies have aimed to better characterize the ^{15}N CSA tensor in peptide bonds and its variability and structural dependence.[21,31−44] However, the degree of intrinsic variability in the ^{15}N CSA tensor remains the subject of considerable debate. Although Hiyama's CSA asymmetry parameter was very different for the two crystal forms, the CSA magnitude ($\Delta\sigma$) was nearly unchanged (−164 vs −161 ppm).[30] Solution relaxation data recorded for ubiquitin pointed to a high degree of variability, but similar data recorded for ribonuclease H, after removal of outliers, indicated a much smaller spread.[35] A subsequent analysis of ubiquitin cross-correlated transverse and longitudinal relaxation data, combined with R_1, R_2, and ^{15}N-{^{1}H} NOE data, indicated a point-to-point variability estimate of only 5.3 ppm, with a 95% confidence interval spanning from 1.4 to 9.4 ppm,[39] even somewhat lower than the spread seen in ribonuclease H,[35] and considerably smaller than the variability reported originally for ubiquitin[33] and more recently for GB3.[44] However, it is important to note that the site-to-site variability hinges on the estimate for the experimental measurement error; the actual best-fitted CSA data show a much larger spread, part of which is attributed to experimental measurement error. A recent elegant study of cross-correlated relaxation data in ubiquitin shows that the extracted CSA values weakly depend on the motional model assumed during the analysis.[40] This ubiquitin study finds a relatively large average CSA asymmetry parameter, η, of 0.28 and notes that an increase in η correlates with a downfield change in the isotropic ^{15}N shift. However, with a Pearson's correlation coefficient, R_P, of 0.36 these tensor parameters showed little correlation with those of Damberg et al.[39] Another recent solid state NMR study utilized slow magic angle spinning to obtain residue-specific ^{15}N and $^{13}C'$ CSA tensors in polycrystalline GB1.[43] That study finds a moderate degree of variability in the magnitude of the CSA tensor (−164 ± 9 ppm) but substantial variations in its asymmetry ($\eta = 0.19 \pm 0.16$), which lack the significant correlation with isotropic shift, previously deduced from solution NMR cross-correlated relaxation studies on ubiquitin.[40]

Here, we use several enhanced NMR techniques to study the ^{15}N CSA of the backbone amides in protein GB3, which has very high sequence and structural similarity to GB1, using both liquid crystal and cross-correlated relaxation NMR. In order to eliminate the effect of a change in solvent conditions between isotropic and aligned samples, we utilize magic angle spinning (MAS) of the same solution to remove the effect of protein alignment,[38,45] thereby allowing the accurate measurement of the small contribution of residual chemical shift anisotropy (RCSA)[41,46−48] on the chemical shifts observed in the liquid crystalline state. These measurements are carried out for six conservative mutants,[49] which align differently with respect to the liquid crystalline matrix consisting of the filamentous bacteriophage Pf1.[47,50] These measurements, as well as the cross-correlated relaxation measurements, are carried out on perdeuterated protein, with the backbone amides back-exchanged to become protonated, thereby removing small effects resulting from remote protons that can interfere with the precise measurement of chemical shifts and relaxation rates. CSA tensors derived in this manner for GB3 result in much improved predictions of the GB3 relaxation rates of ^{15}N-{^{2}H} groups, compared to using a uniform CSA tensor, thereby validating the accuracy of the results derived by our approach.

Materials and Methods

Sample Expression and Purification. Six $^{15}N/^{13}C/^{2}H$ labeled mutants of the 56-residue third IgG-binding domain of protein G, GB3, were made by expression in *Escherichia coli* BL21 (DE3*) cells, transformed with a pET-11 vector containing the mutated GB3 gene. These include K19AV42ED47K, T11KK19AV42E, K19ED40NV42E, K4AK19EV42E, K4AK19EV42E-N-His_6, and K4AK19EV42E-C-His_6. Preparations were grown in M9 minimal media, containing $^{15}NH_4Cl$ and uniformly ^{13}C-enriched glucose (3 g/L), as well as 1 g/L $^{15}N/^{13}C$ Celtone growth medium (Martek Biosciences, Columbia, MD). A high level (∼85%) of deuteration of the nonexchangeable protons was achieved by using 99% D_2O during the entire process. Protein expression was induced by 0.5

(22) Gu, Z. T. T.; Opella, S. J. *J. Magn. Reson.* **1999**, *140*, 340–346.
(23) Marassi, F. M.; Opella, S. J. *J. Magn. Reson.* **2000**, *144*, 150–155.
(24) Opella, S. J.; Marassi, F. M. *Chem. Rev.* **2004**, *104*, 3587–3606.
(25) Pervushin, K.; Riek, R.; Wider, G.; Wuthrich, K. *Proc. Natl. Acad. Sci. U.S.A.* **1997**, *94*, 12366–12371.
(26) Dellwo, M. J.; Wand, A. J. *J. Am. Chem. Soc.* **1989**, *111*, 4571–4578.
(27) Kay, L. E.; Torchia, D. A.; Bax, A. *Biochemistry* **1989**, *28*, 8972–8979.
(28) Peng, J. W.; Wagner, G. *J. Magn. Reson.* **1992**, *98*, 308–332.
(29) Tjandra, N.; Wingfield, P.; Stahl, S.; Bax, A. *J. Biomol. NMR* **1996**, *8*, 273–284.
(30) Hiyama, Y.; Niu, C. H.; Silverton, J. V.; Bavoso, A.; Torchia, D. A. *J. Am. Chem. Soc.* **1988**, *110*, 2378–2383.
(31) Lumsden, M. D.; Wu, G.; Wasylishen, R. E.; Curtis, R. D. *J. Am. Chem. Soc.* **1993**, *115*, 2825–2832.
(32) Fushman, D.; Cowburn, D. *J. Am. Chem. Soc.* **1998**, *120*, 7109–7110.
(33) Fushman, D.; Tjandra, N.; Cowburn, D. *J. Am. Chem. Soc.* **1998**, *120*, 10947–10952.
(34) Lee, D. K.; Wittebort, R. J.; Ramamoorthy, A. *J. Am. Chem. Soc.* **1998**, *120*, 8868–8874.
(35) Kroenke, C. D.; Rance, M.; Palmer, A. G. *J. Am. Chem. Soc.* **1999**, *121*, 10119–10125.
(36) Boyd, J.; Redfield, C. *J. Am. Chem. Soc.* **1999**, *121*, 7441–7442.
(37) Cornilescu, G.; Bax, A. *J. Am. Chem. Soc.* **2000**, *122*, 10143–10154.
(38) Kurita, J.; Shimahara, H.; Utsunomiya-Tate, N.; Tate, S. *J. Magn. Reson.* **2003**, *163*, 163–173.
(39) Damberg, P.; Jarvet, J.; Graslund, A. *J. Am. Chem. Soc.* **2005**, *127*, 1995–2005.
(40) Loth, K.; Pelupessy, P.; Bodenhausen, G. *J. Am. Chem. Soc.* **2005**, *127*, 6062–6068.
(41) Burton, R. A.; Tjandra, N. *J. Biomol. NMR* **2006**, *35*, 249–259.
(42) Wylie, B. J.; Franks, W. T.; Rienstra, C. M. *J. Phys. Chem. B* **2006**, *110*, 10926–10936.
(43) Wylie, B. J.; Sperling, L. J.; Frericks, H. L.; Shah, G. J.; Franks, W. T.; Rienstra, C. M. *J. Am. Chem. Soc.* **2007**, *129*, 5318–5319.
(44) Hall, J. B.; Fushman, D. *J. Am. Chem. Soc.* **2006**, *128*, 7855–7870.
(45) Grishaev, A.; Yao, L. S.; Ying, J. F.; Pardi, A.; Bax, A. *J. Am. Chem. Soc.* **2009**, *131*, 9490–9492.
(46) Sanders, C. R.; Hare, B. J.; Howard, K. P.; Prestegard, J. H. *Prog. Nucl. Magn. Reson. Spectrosc.* **1994**, *26*, 421–444.
(47) Cornilescu, G.; Marquardt, J. L.; Ottiger, M.; Bax, A. *J. Am. Chem. Soc.* **1998**, *120*, 6836–6837.
(48) Hansen, A. L.; Al-Hashimi, H. M. *J. Magn. Reson.* **2006**, *179*, 299–307.
(49) Yao, L. S.; Bax, A. *J. Am. Chem. Soc.* **2007**, *129*, 11326–11327.
(50) Hansen, M. R.; Mueller, L.; Pardi, A. *Nat. Struct. Biol.* **1998**, *5*, 1065–1074.

mM IPTG. Cultures were centrifuged and resuspended in 20 mL PBS buffer. The cells were lysed by heating to 80 °C for 10 min and centrifuged again. The supernatant was loaded on a Superdex 75 HiLoad 26/60 (Amersham Biosciences) column, equilibrated with NMR buffer (25 mM sodium phosphate, 50 mM NaCl, 0.05% w/v NaN_3, pH 6.5).

For measurement of the residual chemical shift anisotropy, mutant GB3 NMR samples contained *ca* 4 mM $^{15}N/^{13}C/^{2}H$ protein and an amount of Pf1 that yielded a suitable degree of alignment for each mutant corresponding to ^{2}H quadrupole splittings of the lock solvent of 16 Hz (K19AV42ED47K), 31 Hz (T11KK19AV42E), 50 Hz (K19ED40NV42E), 56 Hz (K4AK19EV42E), 18 Hz (K4AK19EV42E-N-His_6), and 40 Hz (K4AK19EV42E-C-His_6). For each mutant, two samples were prepared from the same Pf1-containing stock solution: one sample in a 300 μL volume Shigemi microcell, the other in a 40 μL volume Bruker magic angle spinning (MAS) rotor. Isotropic samples at concentrations of 0.8 mM for K4AK19EV42E and 4.0 mM for K19AV42ED47K $^{15}N/^{13}C/^{2}H$ were prepared and used to measure cross-correlated relaxation rates between ^{15}N CSA and $^{15}N-^{13}C'$ dipolar, as well as between ^{15}N CSA and $^{15}N-^{1}H^{N}$ dipolar mechanisms. A sample of 2.5 mM T11KK19EV42E $^{13}C/^{15}N$-GB3 dissolved in 100% D_2O buffer containing 13 mM sodium phosphate, pH 6.9, and 25 mM NaCl was used to measure the R_1 and $R_{1\rho}$ relaxation rates of backbone amide $^{15}N-\{^{2}H\}$ moieties.

NMR Spectroscopy. All NMR experiments were carried out on Bruker Avance 500, 600, and 800 MHz spectrometers, equipped with *z*-axis gradient, triple resonance, cryogenic probeheads and on a Bruker Avance 600 MHz spectrometer equipped with a room-temperature MAS probehead that included a *z*-axis gradient coil. All experiments were performed at 298 K unless explicitly stated.

A three-dimensional HNCO spectrum was recorded for each $^{15}N/^{13}C/^{2}H$-labeled aligned sample. In order to obtain simultaneously the chemical shifts and the one-bond $^{15}N-^{1}H$ and $^{13}C'-^{13}C^{\alpha}$ splittings, which were used to determine the alignment tensors, the HNCO experiments were performed (at 500 MHz ^{1}H frequency) in the absence of ^{1}H decoupling during ^{15}N evolution, and with $^{13}C^{\alpha}$ decoupling omitted during $^{13}C'$ evolution. The acquisition times were 112 ($^{13}C'$), 90 (^{15}N), and 64 ms (^{1}H) with the data matrices consisting of 56* × 128* × 512* data points, where *N** indicates *N* complex points. In these 3D HNCO spectra, each correlation was split into four multiplet components, separated by $^{1}J_{HN} + {}^{1}D_{HN}$ in the ^{15}N dimension and by $^{1}J_{C'C\alpha} + {}^{1}D_{C'C\alpha}$ in the $^{13}C'$ dimension. The frequencies of the four components were averaged to obtain the chemical shift, $\delta_{aligned}$, in the liquid crystalline phase. The isotropic chemical shifts, $\delta_{isotropic}$, for each mutant were obtained from a regular HNCO experiment with heteronuclear decoupling in all dimensions, carried out on the samples under MAS conditions, spinning at a slow rate of ~620 Hz which effectively removed alignment. For several samples, spinning at higher rates (ca. 3 kHz) resulted in the absence of a ^{2}H solvent quadrupole splitting after the MAS spinner was stopped following several days of spinning, presumably due to precipitation of the Pf1 under the relatively high g forces operative under these conditions. Following slower (620 Hz) MAS conditions, no such loss of quadrupole splitting was observed. The acquisition times for the 3D HNCO experiments were 94 ($^{13}C'$), 94 (^{15}N), and 106 ms (^{1}H) with the data matrix consisting of 47* × 94* × 1024* data points. The effect of very small temperature differences between the static and MAS samples on the difference in chemical shift for any given mutant was accounted for during data analysis by measurement of the temperature coefficients of each nucleus, which allowed for an accurate estimate of the difference in effective sample temperatures between aligned and isotropic samples (to within ~0.1 °C), and subsequent removal of the temperature dependent contribution. The temperature coefficients of the $^{1}H^{N}$, ^{15}N, and $^{13}C'$ nuclei were derived from HNCO experiments carried out on mutant K19AV42ED47K in an isotropic solution at 298 K and at 306 K, and these temperature coefficients (SI Table S1) were assumed to be the same for all six mutants. The residual chemical shift anisotropy (RCSA) is then derived from the difference between the chemical shifts measured for the aligned and MAS samples, after the above-mentioned correction for minor differences in temperature.

^{15}N relaxation rates were measured for the mutant K4AK19EV42E, including longitudinal (R_1), spin-locked transverse ($R_{1\rho}$), transverse ^{15}N CSA/N−H dipolar cross-correlated ($\Gamma^{CSA,NH}$), and transverse ^{15}N CSA/N−C′ dipolar cross-correlated ($\Gamma^{CSA,NC'}$) relaxation, using the set of experiments described below, all based on the ^{1}H-detected $^{1}H-^{15}N$ HSQC pulse sequence,[51] and closely related to experiments by Loth et al.[40]

For the $R_{1\rho}$ measurement, carried out using standard methods[52] at 600 MHz ^{1}H frequency, spin-lock durations were 3, 10, 40, 80, 120, 150, 175, and 200 ms. A ^{15}N spin-lock field strength of 2.4 kHz was used with the carrier frequency positioned in the center of the ^{15}N spectrum. A single ^{1}H composite pulse $90°_x-210°_y-90°_x$ was applied at the midpoint of the spin-lock period to suppress the effect of ^{15}N CSA/N−H dipolar cross-correlation. A 500 μs hyperbolic secant 180° $^{13}C'/^{13}C^{\alpha}$ pulse[53] was utilized in a similar way to suppress ^{15}N CSA/N−C′ as well as ^{15}N CSA/N−C^{α} dipolar cross-correlation. The acquisition times were 80 (^{15}N) and 61 ms (^{1}H), with the data matrices consisting of 160* × 512* points. A 2-s water saturation pulse with a RF field strength of 37 Hz was applied during the delay between scans, and ^{15}N RF heating compensation pulses were utilized to ensure the temperature of the $R_{1\rho}$ experiment to remain constant.[54]

For the R_1 measurement, carried out at 600 MHz ^{1}H frequency, the longitudinal relaxation delays were 50.6, 151.8, 253, 354.2, 455.4, and 506 ms. A ^{1}H composite pulse $90°_x-210°_y-90°_x$ and a hyperbolic secant 180° ^{13}C pulse were applied every 50 ms during the R_1 relaxation delay to remove the effect of longitudinal ^{15}N CSA/N−H^{N} and ^{15}N CSA/ C′(C^{α}) dipolar cross-correlation. The acquisition times were 56 (^{15}N) and 80 (^{1}H) ms, with data matrices consisting of 140* × 768* points.

Transverse ^{15}N CSA/N−H^{N} dipolar cross-correlated relaxation rates, $\Gamma^{CSA,NH}$, were measured using a constant-time ^{15}N evolution HSQC experiment (Supporting Information, Figure S2). This experiment, and the analogous measurement of the ^{15}N CSA/N−C′ dipolar cross-correlated relaxation rates, $\Gamma^{CSA,NC'}$, are based on measurement of the relative intensities of ^{15}N doublet components after a constant-time evolution period lacking ^{1}H (or $^{13}C'$) decoupling, and are fully analogous to methods described previously for this purpose[55,56] (SI Figure S2). The value of $\Gamma^{CSA,NH}$ then directly follows from the intensity ratio of the up- and downfield components of the ^{15}N doublets.[55,56] The $\Gamma^{CSA,NH}$ measurement was performed at 600 MHz ^{1}H frequency using constant-time durations 2T of 81.6 and 161.6 ms, and at 500 MHz with 2T 81.6 ms. The delay between scans was 1.5 s. The $\Gamma^{CSA,NC'}$ dipolar cross-correlated relaxation rate was measured in the same way, but with the pulse sequence modified to decouple ^{1}H during constant-time ^{15}N evolution by means of two composite $90°_x-210°_y-90°_x$ ^{1}H pulses, and to decouple $^{13}C^{\alpha}$ and other aliphatic carbons by using two band-selective 2.0-ms hyperbolic secant 180° pulses[53] during ^{15}N constant-time evolution (Figure S3). The experiment was carried out at both 500 and 600 MHz ^{1}H frequency, using a constant-time duration, 2T, of 165.1 ms. Resonance overlap was observed for the correlations of E24 and T25 in the ^{15}N-CSA/N−H^{N} dipolar cross-correlated relaxation spectrum. To solve this problem, a ^{15}N-CSA/N−H^{N} cross-correlated experiment (at 600 MHz) was performed on the K19AV42ED47K mutant, where these resonances are slightly shifted relative to one another, using a constant-time

(51) Bodenhausen, G.; Ruben, D. J. *Chem. Phys. Lett.* **1980**, *69*, 185–189.
(52) Mulder, F. A. A.; de Graaf, R. A.; Kaptein, R.; Boelens, R. *J. Magn. Reson.* **1998**, *131*, 351–357.
(53) Silver, M. S.; Joseph, R. I.; Hoult, D. I. *Nature* **1984**, *310*, 681–683.
(54) Wang, A. C.; Bax, A. *J. Biomol. NMR* **1993**, *3*, 715–720.
(55) Fischer, M. W. F.; Zeng, L.; Pang, Y. X.; Hu, W. D.; Majumdar, A.; Zuiderweg, E. R. P. *J. Am. Chem. Soc.* **1997**, *119*, 12629–12642.
(56) Tjandra, N.; Bax, A. *J. Am. Chem. Soc.* **1997**, *119*, 8076–8082.

duration 2T of 81.6 ms. By linearly fitting the rates of residues measured for K4AK19EV42E to those measured for the five times more concentrated sample of K19AV42ED47K, a scaling factor of 1.086 was determined with a Pearson's correlation coefficient $R_P = 0.993$, allowing the $\Gamma^{CSA,NH}$ rates of E24 and T25 to be taken from this second measurement.

Longitudinal (R_1) and spin-locked transverse ($R_{1\rho}$) ^{15}N relaxation rates were also measured for the mutant T11KK19EV42E dissolved in 100% D_2O, using a modified HA(CACO)N sequence[57] (SI Figure S4). The R_1 measurement was performed at 600 MHz ^{1}H frequency with delays of 0.101, 0.303, 0.505, 0.707, 0.808, 0.909, and 1.01s, and at 800 MHz field with delays of 0.050, 0.100, 0.300, 0.501, 0.701, 0.901, and 1.00 s. R_1 experiments were performed at 283 K. The $R_{1\rho}$ was measured at 600 MHz ^{1}H frequency, using a spin lock field strength of 2.0 kHz, and carried out both at 283 K and at 298 K, in order to identify residues affected by temperature-dependent conformational exchange.

All spectra were processed and analyzed using the software package NMRPipe.[58] Peak positions and intensities were determined by parabolic interpolation. R_1 and $R_{1\rho}$ rates were determined from two-parameter exponential fits of peak intensities. The R_2 rate was calculated by eliminating the R_1 contribution from the measured $R_{1\rho}$ rate.[59] The cross-correlated relaxation rates Γ were calculated from the intensity ratio of the up- and downfield ^{15}N doublet components.[56]

Quantum Chemical Calculations. The model compound N-methyl acetamide (NMA) was used to calculate the difference in the effective length of N−D and N−H bonds. The molecular geometry was optimized using the Gaussian 03 program for B3LYP/6-31G** density functional calculations in a continuum solvent model (dielectric constant 78.4).[60] To explore the ^{15}N CSA differences between α-helix and β-strand conformations, alanine dipeptide models ($HCO(NHCH(CH_3)CO)_2H$) were built with backbone ϕ, Ψ angles set equal to typical α-helix (T25-A26) and β-strand (F52-T53) conformations of the NMR-refined X-ray structure (PDB entry 2OED).[61] One alanine dipeptide model was also built with ϕ, Ψ angles corresponding to T49-K50 while another Ala-Gly model was built with ϕ, ψ angles equal to those of N37-G38. The models were optimized at the B3LYP/6-311+G** level while keeping all the dihedral angles fixed, and the chemical shielding tensors were calculated using the GIAO method[62,63] at the B3LYP/aug-cc-pvtz level. The chemical shift tensor was computed as $\delta_{ii} = \delta_0 - \sigma_{ii}$ ($i = X, Y, Z$), where δ_0 is 244.6 ppm, the absolute chemical shift of liquid ammonia at 298 K, and σ_{ii} are the calculated CSA tensor principal components.

Results

Theoretical Background. The change in chemical shift for a given nucleus upon switching from the isotropic to the liquid crystalline phase is commonly referred to as the residual chemical shift anisotropy, or RCSA, and is given by

$$\Delta\delta = -\frac{2}{3}[\langle P_2(\cos\theta_1)\rangle\sigma_{XX} + \langle P_2(\cos\theta_2)\rangle\sigma_{YY} + \langle P_2(\cos\theta_3)\rangle\sigma_{ZZ}] \quad (1)$$

where $P_2(\alpha) = (3\alpha^2-1)/2$, σ_{XX}, σ_{YY}, and σ_{ZZ} are the principal components of the traceless CSA tensor, while θ_1, θ_2, and θ_3 are the angles between the principal axes of the CSA tensor and the magnetic field orientation. The angular brackets, $\langle ... \rangle$, refer to ensemble averaging. By applying the spherical harmonics addition theorem, eq 1 can be rewritten as

$$\Delta\delta = -\frac{2}{3}[\langle b_1\rangle\sigma_{XX} + \langle b_2\rangle\sigma_{YY} + \langle b_3\rangle\sigma_{ZZ}]\langle a\rangle \quad (2)$$

where b and a are vectors of the same form

$$b_i = \left\{(3z_i^2 - 1)/2, \frac{\sqrt{3}}{2}(x_i^2 - y_i^2), \sqrt{3}x_iz_i, \sqrt{3}y_iz_i, \sqrt{3}x_iy_i\right\}, \text{ with } i = 1-3 \quad (3a)$$

$$a = \left\{(3z^2 - 1)/2, \frac{\sqrt{3}}{2}(x^2 - y^2)\sqrt{3}xz, \sqrt{3}yz, \sqrt{3}xy\right\} \quad (3b)$$

where (x_i, y_i, z_i) are the Cartesian coordinates of the CSA principal axis b_i and (x, y, z) are the Cartesian coordinates of the magnetic field in the molecular frame, and $\langle a\rangle$ represents the alignment tensor. If internal motion is assumed to be isotropic and affects all three CSA principal components in the same way, a single order parameter is sufficient to describe such motion. Equation 2 then can be rewritten as

$$\Delta\delta = -\frac{2}{3}S^{RCSA}[b_1\sigma_{XX} + b_2\sigma_{YY} + b_3\sigma_{ZZ}]\langle a\rangle \quad (4)$$

where S^{RCSA} is the order parameter. Assuming a uniform order parameter for the backbone amide ^{15}N nuclei in the highly ordered regions of GB3, eq 4 can be rewritten in matrix format for the case where RCSAs are measured under N different alignment tensors

$$\Lambda = -\frac{2}{3}S^{RESA}[\mathbf{B}_{\sigma_{XX}} + \mathbf{B}_{\sigma_{YY}} + \mathbf{B}_{\sigma_{ZZ}}]\langle\mathbf{A}\rangle \quad (5)$$

where $\mathbf{\Lambda}$ is a $L \times N$ matrix, $\mathbf{B}_{oii}$ (i = X, Y, Z) is a $L \times 5$ matrix, $\langle\mathbf{A}\rangle$ is a $5 \times N$ matrix and L is the number of nuclei. ^{15}N−^{1}H RDCs measured under multiple alignments can be expressed as[64]

$$\mathbf{D}_M = D_{max}^{NH}\langle\mathbf{B}\rangle\langle\mathbf{A}\rangle \quad (6)$$

where $\mathbf{D}_M$ is the $L \times N$ RDC matrix and $\mathbf{B}$ is an $L \times 5$ matrix, each row of which is a dipole internuclear vector of the same form as b described earlier and $\langle\mathbf{A}\rangle$ is the alignment matrix. D_{max}^{NH} is a constant, defined as

$$D_{max}^{NH} = -\mu_0\hbar\gamma_N\gamma_H\langle r_{NH}^{-3}\rangle/4\pi^2 \quad (7)$$

where $\mu_0$is the magnetic permittivity of vacuum, $\hbar$is the reduced Planck's constant, γ_H is the ^{1}H gyromagnetic ratio, r_{NH} is the internuclear distance, and $\langle ... \rangle$ denotes averaging over the zero-point vibrational motion (including N−H bond stretching and librational motions). In our earlier study, using multiple RDCs in six alignments, we found $r_{eff} = \langle r_{NH}^{-3}\rangle^{-1/3} = 1.015$ Å when only considering the bond stretching motion.[65] In addition,

(57) LiWang, A. C.; Bax, A. *J. Magn. Reson.* **1997**, *127*, 54–64.
(58) Delaglio, F.; Grzesiek, S.; Vuister, G. W.; Zhu, G.; Pfeifer, J.; Bax, A. *J. Biomol. NMR* **1995**, *6*, 277–293.
(59) Davis, D. G.; Perlman, M. E.; London, R. E. *J. Magn. Reson. Ser. B* **1994**, *104*, 266–275.
(60) Frisch, M. J.; et al.; *Gaussian 03*, revision C.02; Gaussian Inc.: Wallingford, CT, 2004.
(61) Ulmer, T. S.; Ramirez, B. E.; Delaglio, F.; Bax, A. *J. Am. Chem. Soc.* **2003**, *125*, 9179–9191.
(62) Ditchfield, R. *Mol. Phys.* **1974**, *27*, 789–807.
(63) Wolinski, K.; Hinton, J. F.; Pulay, P. *J. Am. Chem. Soc.* **1990**, *112*, 8251–8260.
(64) Yao, L.; Vogeli, B.; Torchia, D. A.; Bax, A. *J. Phys. Chem. B* **2008**, *112*, 6045–6056.
(65) Yao, L.; Voegeli, B.; Ying, J. F.; Bax, A. *J. Am. Chem. Soc.* **2008**, *130*, 16518–16520.

quantum calculations for the model compound *N*-methylacetamide (NMA) indicate that the zero-point librational motions reduce the ^{15}N−^{1}H dipolar coupling by 7.6%, equivalent to lengthening the effective bond by 0.025 Å to $r_{eff} = 1.040$ Å.[65,66] By assuming a group of residues with only isotropic motions of uniform amplitude, described by an order parameter S^{RDC}, eq 6 can be written as

$$\mathbf{D}_M = \mathbf{B}\mathbf{A}mat \tag{8}$$

with the apparent alignment matrix $\mathbf{A}mat$ given by

$$\mathbf{A}mat = -\mu_0\hbar\gamma_N\gamma_H r_{eff}^{-3} S^{RDC}\langle\mathbf{A}\rangle/4\pi^2 \tag{9}$$

The alignments, $\mathbf{A}mat$, can be determined from the RDCs, by means of either singular value decomposition (SVD) if atomic coordinates are known[67] or if coordinates are unknown but three or more alignment orientations are available, by direct interpretation of dipolar couplings (DIDC),[64,68] or by other approaches that minimize the alignment error caused by structural noise.[69] As seen from eq 9, knowledge of $S^{RDC}r_{eff}^{-3}$ is prerequisite for determining the $\langle\mathbf{A}\rangle$ matrix, and therefore for determining the CSA tensor (eqs 4,5). Entering the r_{eff} value and those of the other constants into eq 9 yields

$$\langle\mathbf{A}\rangle = 4.617 \times 10^{-5}\mathbf{A}mat/S^{RDC} \tag{10}$$

As seen from eq 10, the absolute amplitude of alignment depends on the motional amplitude of the N−H bond vectors. Equation 5 then can be rewritten as

$$\mathbf{\Lambda} = -(-3.078 \times 10^{-5} S^{RCSA}/S^{RDC})\lfloor \mathbf{B}_{\sigma_{XX}} + \mathbf{B}_{\sigma_{YY}} + \mathbf{B}_{\sigma_{ZZ}}\rfloor \mathbf{A}mat \tag{11}$$

where $\mathbf{\Lambda}$ represents the experimental RCSA values, and $\mathbf{A}mat$ is obtained from RDCs, as described above. Therefore S^{RCSA}/S^{RDC} $\mathbf{B}_{\sigma_{ii}}$ (i = X, Y, Z) follows from eq 11. The apparent CSA tensor for a given nucleus, obtained from RCSAs, scales relative to the static CSA tensor according to

$$\sigma_{ii}^{app\_RCSA} = \sigma_{ii} S^{RCSA}/S^{RDC} \ (i = X,Y,Z) \tag{12}$$

Information on the ^{15}N CSA tensor can also be derived from relaxation data, in particular the R_1, R_2, and the CSA/dipolar cross-correlated relaxation rate $\Gamma^{CSA,DD}$. It is well recognized that zero-point backbone motions scale down both the N−H dipole interaction and the ^{15}N CSA, σ_{ii}. However the applicable scaling factors (order parameters caused by zero point motions) for the two types of interactions are different, with the ^{15}N CSA rescaling resulting from such motions being much weaker than that for the dipolar interaction, and the scaling of $\Gamma^{CSA,DD}$ falling in between.[70] It is also worth noting that the scaling due to zero point motions of $\Gamma^{CSA,DD}$ for ^{15}N CSA and N−C′ dipole cross-correlation is complicated by the large angle between the main principal axis of the nearly axially symmetric ^{15}N CSA tensor, σ_{ZZ}, and the N−C′ bond vector (ca. 100°). This intrinsic complexity can be greatly reduced if the zero-point motion of the entire peptide plane, which may be assumed to be quite uniform and very small for all peptide bonds, is excluded from the relaxation data analysis. For isotropic internal motion, the dipole−dipole order parameter will be the same as the CSA order parameter in both relaxation and RCSA data analysis, i.e., S^{RCSA}/S^{RDC} and $S_{CSA}^{rel} = S_{DD}^{rel}$ (order parameters derived from relaxation for CSA and dipole tensors), and the cross-correlated relaxation rate $S_{CSA-DD}^{rel} = (S_{CSA}^{rel} = S_{DD}^{rel})^{1/2} = S_{DD}^{rel}$. As a result, the ^{15}N CSA σ_{ii} value determined in this study $\sigma_{ii} = \sigma_{ii}^{app\_RCSA} = \sigma_{ii}^{app\_rel}$ corresponds to the effective CSA averaged over zero-point motions, equivalent to what would be measured in a static solid-state NMR experiment in the absence of thermally activated motions, i.e., for a sample temperature approaching 0 K.

The ^{15}N CSA and N−H (or N−C′) dipole cross-correlated relaxation rate for an isotropically tumbling system is described by[71]

$$\Gamma = -\frac{\mu_0\hbar\gamma_N^2\gamma_A\mathbf{B}_0}{60\pi r_{eff}^3}(\sigma_{XX}P_2(\cos\alpha_1) + \sigma_{YY}P_2(\cos\alpha_2) + \sigma_{ZZ}P_2(\cos\alpha_3))\{4J(\omega_N)\} \tag{13}$$

where $\mathbf{B}_0$ is the magnetic field strength, the subscript A represents the second nucleus, H or C′, and α_1, α_2, and α_3 are angles between the N−H or N−C′ bond vector and the X, Y, Z principal axes of the ^{15}N CSA tensor, respectively. The N−C′ bond length of 1.329 Å is accurately known from high resolution X-ray structures on small peptides.[72]

R_1 and R_2 relaxation rates also are affected by CSA and therefore carry information on its magnitude. However, at the commonly used magnetic field strength of 14.1 T (600 MHz ^{1}H frequency), the CSA relaxation mechanism is much smaller than the ^{15}N−^{1}H dipolar contribution and accounts for only ∼27% of the R_1 and R_2 rates.[73] Thus, these rates are dominated by the ^{15}N−^{1}H dipolar interaction. The fractional contribution of CSA to the relaxation rate can be greatly increased by exchanging the amide protons for deuterons, simply accomplished by dissolving the protein sample in 100% D_2O. Due to the smaller magnetogyric ratio of ^{2}H compared to ^{1}H, its dipolar contribution to ^{15}N relaxation is greatly diminished and the relative effect of CSA on ^{15}N relaxation therefore is considerably larger for ^{15}N−{^{2}H} groups. To increase the otherwise very slow and more difficult to measure transverse relaxation rates of ^{15}N−{^{2}H} groups, the rotational correlation time can be increased by lowering the temperature (to 283 K in this study). The R_1 and R_2 relaxation rates for ^{15}N−{^{2}H} in an isotropically tumbling system are described by Goldman (1984)

$$R_1 = -\frac{\mu_0^2\hbar^2\gamma_N^2\gamma_D^2}{60\pi^2 r_{eff}^6}\{J(\omega_D - \omega_N) + 3J(\omega_N) + 6J(\omega_D + \omega_N)\} + 6c^2J(\omega_N) + R_{1P} \tag{14}$$

$$R_2 = -\frac{\mu_0^2\hbar^2\gamma_N^2\gamma_D^2}{120\pi^2 r_{eff}^6}\{4J(0) + J(\omega_D - \omega_N) + 3J(\omega_N) + 6J(\omega_D) + 6J(\omega_D + \omega_N)\} + C^2\{4J(0) + 3J(\omega_N)\} + R_{2P} + R_{ex} \tag{15}$$

where $c^2 = (1/45)(\gamma_N B_0)^2(\sigma_{XX}^2 + \sigma_{YY}^2 + \sigma_{ZZ}^2 - \sigma_{XX}\sigma_{YY} - \sigma_{XX}\sigma_{ZZ} - \sigma_{YY}\sigma_{ZZ})$. R_{1p} and R_{2p} are the dipolar relaxation contributions

(66) Case, D. A. *J. Biomol. NMR* **1999**, *15*, 95–102.
(67) Losonczi, J. A.; Andrec, M.; Fischer, M. W. F.; Prestegard, J. H. *J. Magn. Reson.* **1999**, *138*, 334–342.
(68) Tolman, J. R. *J. Am. Chem. Soc.* **2002**, *124*, 12020–12030.
(69) Lakomek, N. A.; Walter, K. F. A.; Fares, C.; Lange, O. F.; de Groot, B. L.; Grubmuller, H.; Bruschweiler, R.; Munk, A.; Becker, S.; Meiler, J.; Griesinger, C. *J. Biomol. NMR* **2008**, *41*, 139–155.
(70) Tang, S.; Case, D. A. *J. Biomol. NMR* **2007**, *38*, 255–266.
(71) Goldman, M. *J. Magn. Reson.* **1984**, *60*, 437–452.
(72) Engh, R. A.; Huber, R. *Acta Crystallogr. A* **1991**, *47*, 392–400.
(73) Hall, J. B.; Fushman, D. *J. Biomol. NMR* **2003**, *27*, 261–275.

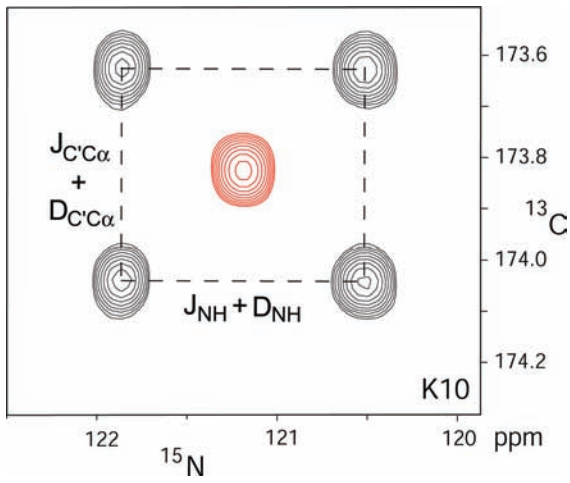

Figure 1. Superposition of $^{13}C-^{15}N$ cross sections taken at the $^{1}H^{N}$ frequency of residue K10 through the HNCO 3D spectra recorded for aligned (black contours) and magic angle spinning (red contours) samples of GB3 mutant K19AV42ED47K. The spectrum on the aligned sample was recorded without $^{13}C^{\alpha}$ decoupling during $^{13}C'$ evolution, and without $^{1}H^{N}$ decoupling during ^{15}N evolution; the isotropic data were recorded in the presence of decoupling, yielding a single resonance.

resulting from nuclei other than the attached ^{2}H, including the adjacent $^{13}C'$ and $^{13}C^{\alpha}$ spins, and remote ^{13}C and ^{1}H nuclei; R_{ex} is the transverse relaxation contribution resulting from conformational exchange. The rotational diffusion tensor of GB3 protein is anisotropic and therefore more general forms of eqs 13−15 are used in this study (SI, eqs S2−S4).

Determination of Alignment Tensors. Each of the six GB3 mutants was aligned in a liquid crystalline suspension of Pf1, adjusted to a concentration that yielded a degree of GB3 alignment that was suitable for measuring $^{15}N-^{1}H$ RDCs at high relative accuracy, with values in the −25 to +45 Hz range. Note that this degree of alignment is somewhat stronger than commonly used for protonated proteins. Together, these six mutants provide a very good mapping of the five-dimensional alignment space.[49] The isotropic chemical shifts, $\delta_{isotropic}$, for each mutant were obtained from a regular HNCO experiment with heteronuclear decoupling in all dimensions, carried out on the samples under MAS conditions, spinning at a slow rate of ~620 Hz which effectively removed alignment (Figure 1). Singular value decomposition (SVD) fitting[67,74] of the experimental RDCs to the N−H orientations obtained in our previous study (SI table S8) was used to determine the alignment tensors, **A***mat*, for each of the six mutants (Table 1). The vector orientations were also used for fitting the relaxation data and the RCSA values, in order to determine the rotational diffusion tensor and the site-specific ^{15}N CSA tensors.

Residual Chemical Shift Anisotropy. Owing to the weak alignment of the protein in the dilute liquid crystalline Pf1 suspension, a small amount of residual chemical shift anisotropy contributes to the observed chemical shifts. Just like the dipolar couplings, the RCSA is scaled down relative to its static CSA value by about 3 orders of magnitude, and RCSA effects for ^{15}N then typically fall in the ±100 ppb range, considerably larger than the estimated RCSA random measurement error of ±5 ppb. Accurate measurement of such small chemical shift differences between isotropic and aligned samples also requires the absence of systematic effects that might perturb these chemical shifts. Such effects may include the difference in solvent composition, including small differences in ionic strength, pH, or molecules associated with the liquid crystalline matrix. These "solvent effects", together with possible small differences in experimental sample temperature between the recordings of the separate spectra, previously were significant concerns in determining highly accurate RCSA values, and a number of methods have been devised to minimize them.[37,41,76] For example, it is relatively easy to generate an isotropic bicelle solution that is similar in composition to the liquid crystalline bicelle sample, causing the effect of the change in medium to nearly cancel. Alternatively, by changing the temperature across the nematic to isotropic phase boundary, the same sample can be studied under isotropic and aligned conditions, but this increases the effect of uncertainty in the temperature coefficients of the chemical shifts.[37] For the highly robust and popular alignment medium of filamentous bacteriophage Pf1,[50] it is not readily possible to introduce a switch between isotropic and aligned phases for a static sample. Instead, we here study two Pf1-containing samples, prepared from the same stock solution with one sample contained in a regular Shigemi NMR microcell and the other in a 4-mm outer diameter magic angle spinning rotor (40 μL volume). Depending on Pf1 concentration and ionic strength, static liquid crystalline Pf1 samples require between seconds and minutes to align once placed in an external magnetic field. Slow spinning around the magic angle axis is therefore efficient at removing magnetic field alignment of the Pf1, analogous to what was used previously for bicelles.[38,77,78] The slowest stable MAS spinning rate achievable on our Bruker NMR probehead was ca. 620 Hz, and this rate was used for measurement of chemical shifts under isotropic conditions. Besides the effect of random noise, the main uncertainty introduced when comparing chemical shifts recorded for the static and MAS samples then relates to small differences in temperature. Temperature control of the MAS probe is relatively crude, and the effective sample temperature was determined a posteriori, in the manner described below, followed by small corrections of these chemical shifts using their experimentally established temperature coefficients (Table S1).

To determine the temperature difference between the aligned and MAS samples, we calculated the $^{1}H^{N}$ RCSA values predicted for a uniform CSA tensor of the magnitude determined

Table 1. Alignment Tensors for the GB3 Mutants in Liquid Crystalline Pf1[a]

	D_a (Hz)	R	α [b]	β[b]	γ [b]
K19AV42ED47K	24.0	0.253	82.7	94.2	294
K19ED40NV42E	−12.4	0.222	89.9	336	133
K4AK19EV42E-C-histag	8.61	0.461	162	258	213
K4AK19EV42E-N-histag	18.5	0.179	123	256	184
T11KK19AV42E	20.0	0.300	102	246	220
K4AK19EV42E	10.3	0.551	162	251	23.0

[a] The RDCs are fitted to the N−H orientations determined previously[65] that were aligned relative to the molecular frame of PDB entry 2OED[61] (SI, Table S8). [b] The angles reported are $z-y-z$ convention Euler angles needed to rotate the molecular frame to the alignment tensor frame.[75]

(74) Sass, J.; Cordier, F.; Hoffmann, A.; Rogowski, M.; Cousin, A.; Omichinski, J. G.; Lowen, H.; Grzesiek, S. *J. Am. Chem. Soc.* **1999**, *121*, 2047–2055.
(75) Spiess, H. W. *NMR Basic Princip. Progr.* **1978**, *15*, 55–214.
(76) Burton, R. A.; Tjandra, N. *J. Am. Chem. Soc.* **2007**, *129*, 1321–1326.
(77) Zandomeneghi, G.; Williamson, P. T. F.; Hunkeler, A.; Meier, B. H. *J. Biomol. NMR* **2003**, *25*, 125–132.
(78) Zandomeneghi, G.; Tomaselli, M.; Williamson, P. T. F.; Meier, B. H. *J. Biomol. NMR* **2003**, *25*, 113–123.

Table 2. Rotational Diffusion Tensor for the K4AK19EV42E Mutant of GB3[a]

D_{XX}[b] ($\times 10^7$ s^{-1})	D_{YY} ($\times 10^7$ s^{-1})	D_{ZZ} ($\times 10^7$ s^{-1})	θ (°)	ϕ (°)
4.67	4.67	6.34	60.3	96.6

[a] Values correspond to 95% H_2O, 5% D_2O at 298 K. The principal components of the diffusion tensor for T11KK19EV42E in 100% D_2O, 283 K, are scaled down by 0.481 relative to values listed for K4AK19EV42E. [b] The D_{XX} and D_{YY} values are restrained to be the same, and θ and ϕ are polar coordinates for the unique axis of the tensor in the coordinate frame of PDB entry 2OED with the N−H orientations defined by our previous RDC analysis[65] (SI, Table S8).

previously[37] for each of the alignment tensors determined above. By plotting the difference between predicted RCSA and experimental values against the proton chemical shift temperature coefficients (SI Figure S5), a precise measure for the temperature difference between the MAS and static samples is obtained, and this procedure will also reveal any potential problems with chemical shift referencing between the two measurements. MAS spectra for the six different mutants were recorded over the time span of more than a year, and differences between the MAS and static sample temperatures ranged from +0.45 to +1.3 °C. The experimental amide ^{15}N RCSA were corrected as follows:

$$\Delta\delta = \Delta\delta_{exp} + c\Delta T + \varepsilon \quad (16)$$

where $\Delta\delta$ and $\Delta\delta_{exp}$ are the corrected and raw RCSA, respectively, c is the ^{15}N linear temperature coefficient (SI Table S1), and ε accounts for small problems with the chemical shift referencing, resulting from the fact that the water resonance position, used for indirect referencing of the ^1H and ^{15}N chemical shifts, can vary with the precise electronic tuning of the cryogenic probehead used;[79] ΔT is the temperature difference as listed in SI Table S2. Based on reproducibility of both the static and MAS ^{15}N chemical shift measurements, the experimental random uncertainty in $\Delta\delta$ is estimated at ±0.3 Hz, or ±5 ppb.

Rotational Diffusion Tensor Determination. The rotational diffusion tensor for the $^2H/^{15}N/^{13}C$-labeled K4AK19EV42E GB3 mutant in H_2O was determined by optimizing its trace, degree of axial asymmetry, and orientation relative to the NMR-refined GB3 structure (PDB entry 2OED)[61] such that it yielded a best fit of the experimental R_2/R_1 ratios. R_2 and R_1 rates were calculated using expressions for both axially symmetric and asymmetric diffusion tensors[75,80,81] but, as found previously,[73,83] the fully asymmetric diffusion tensor did not result in an improvement of the fit that statistically warranted the introduction of two additional parameters needed to describe this deviation from axial symmetry. The dipolar contributions from all atoms within 4 Å from the ^{15}N nucleus were included in these R_2 and R_1 rate calculations. Although to first order the results are insensitive to the precise values of the CSA tensor components and N−H-bond length, uniform values based on a previous best estimate of (−109, 46, 63 ppm and 19° β angle) for the CSA tensor[37] and 1.040 Å for the zero-point motion adjusted effective N−H bond length[65] were used.

The thus obtained diffusion tensor values (Table 2), corresponding to an effective rotational correlation time $t_c = 3.19$ ns and a diffusion anisotropy of $D_{//}/D_{-} = 1.36$, are in close agreement with results reported previously[73,82] and yield an excellent correlation between observed and predicted R_2/R_1 ratios ($R_P = 0.97$; Figure S6). The diffusion tensor parameters are essentially indistinguishable from results obtained when using the analytic equations developed for the axially symmetric diffusion tensor[83] (data not shown).

The rotational diffusion tensor asymmetry and principal axes orientations of the $^{15}N/^{13}C$-labeled mutant T11KK19EV42E in D_2O at 283 K were assumed to be the same as those in H_2O, but the tumbling time under these higher viscosity conditions is much longer, and only the trace of the diffusion tensor was treated as a variable in the fit of the $^{15}N-^2H$ relaxation rates. Best fitting of the $^{15}N-\{^2H\}$ R_1 and R_2 rates, while excluding residues for which the temperature dependence of R_2 was indicative of an exchange broadening process (see below), yielded an effective correlation time of 6.63 ns (see SI for details). This value is somewhat larger than the value of 5.94 ns expected on the basis of the increased viscosity at this lower temperature of D_2O, comparing to the value of 3.19 ns measured at 25 °C in H_2O. The longer correlation time is likely caused by the higher protein concentration of the sample used in D_2O (2.5 mM) than in H_2O (0.8 mM). In fact, if the prediction were based on relaxation data measured for another mutant (K19AD47K) at 4.0 mM, an effective correlation time of 6.43 ns was obtained. When deriving the rotational correlation time from five residual amide $^{15}N-^1H$ sites (E27, F30, T44, T51, and F52) in T11KK19EV42E, whose protons had not back-exchanged to ^2H after several weeks, a restrained fit of their R_2/R_1 ratios (keeping the orientation and asymmetry of the diffusion tensor again fixed at the values measured in H_2O solution) yields $\tau_c = 6.5 \pm 0.2$ ns.

Cross-Correlated Relaxation Rates. The ^{15}N CSA/N−H dipole cross-correlation rates, $\Gamma^{CSA,NH}$, were measured at 600 MHz ^1H frequency from the relative $^{15}N-\{^1H\}$ doublet intensities, obtained in a constant-time $^1H-^{15}N$ HSQC experiment (Figure S2, S10). Analysis of data recorded with constant-time evolution periods of 81.6 and 161.6 ms yielded essentially the same rates (SI Figure S7). The $\Gamma^{CSA,NH}$ cross-correlation rates were also measured at 500 MHz ^1H frequency, using a 81.6 ms constant-time duration. The rates derived from the measurements at the two fields correlate very well with each other (Pearson's correlation coefficient $R_P = 0.99$) and the slope of 0.87 falls very close to the theoretical value of 0.88 calculated for a protein with a tumbling time of 3.19 ns (Figure 2A). Based on the pairwise root-mean-square deviation (rmsd) from the expected linear correlation, the error in the 600 MHz cross correlation rates was estimated to be ~0.05 s^{-1}, i.e., <2% of the observed rates. As described in the Materials and Methods section, due to peak overlap the cross-correlated relaxation rates of E24 and T25 were measured from a different mutant, K19AV42ED47K, and scaled by 1.086 to account for tumbling time differences between the samples. The need for a scaling factor raises the concern that transient intermolecular interactions in this mutant, responsible for the apparent increase in rotational correlation time, could also impact the diffusion tensor anisotropy and orientation. However the rmsd between the ^{15}N CSA/$^{15}N-^1H$ $\Gamma^{CSA,DD}$ values measured for the two samples (after rescaling by 1.086) equals 0.05 s^{-1} and therefore is completely dominated by the experimental error. This indicates that the impact of

(79) Torchia, D. A. *J. Biomol. NMR* **2009**, in press.
(80) Woessner, D. E. *J. Chem. Phys.* **1962**, *36*, 1–4.
(81) Ying, J. F.; Grishaev, A. E.; Bax, A. *Magn. Reson. Chem.* **2006**, *44*, 302–310.
(82) Stone, M. J.; Gupta, S.; Snyder, N.; Regan, L. *J. Am. Chem. Soc.* **2001**, *123*, 185–186.
(83) Fushman, D.; Xu, R.; Cowburn, D. *Biochemistry* **1999**, *38*, 10225–10230.

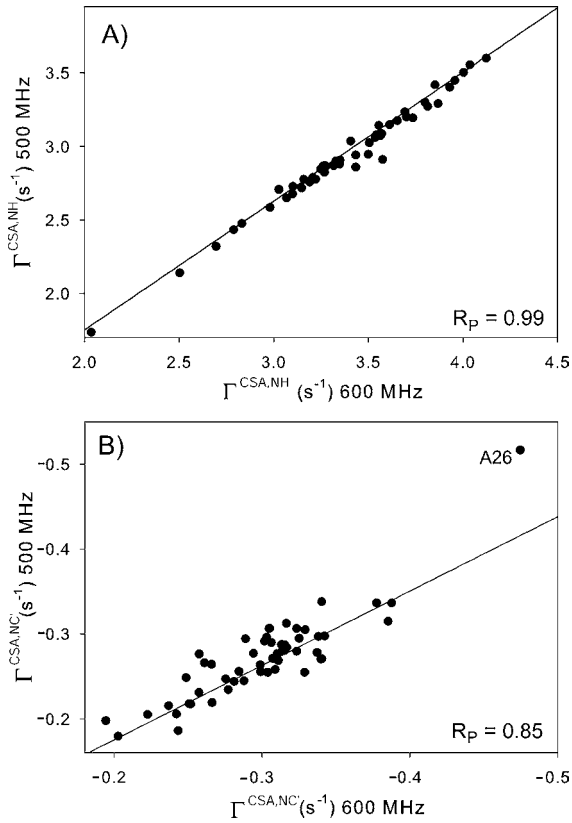

Figure 2. Correlation of transverse ^{15}N CSA/^{15}N−^{1}H dipole cross-correlation rates (A) and transverse ^{15}N CSA/^{15}N−^{13}C′ dipole cross-correlation rates (B), measured at 500 and 600 MHz ^{1}H frequency. The solid lines correspond to the theoretical rate ratio of 0.88 for a 3.19 ns tumbling time. The outlier value measured for A26 in (B) is not included in the calculation of R_P.

transient intermolecular interactions on the diffusion tensor orientation and anisotropy falls well below the detection limit of our measurements.

The ^{15}N CSA/N−C′ dipole cross-correlation rates, $\Gamma^{CSA,NC'}$, measured at both 600 and 500 MHz ^{1}H frequency using the constant-time HSQC experiment of Figure S3, are much smaller than the $\Gamma^{CSA,NH}$ rates and therefore show considerably more scatter (R_P = 0.85). However, the slope of 0.90 agrees well within experimental error with the ratio of 0.88 expected for a molecule tumbling with τ_c = 3.19 ns (Figure 2B). Based on the scatter observed in Figure 2B, the random measurement error was estimated to be 0.02 s^{-1}, or 5−10% of the observed rates. Outlier $\Gamma^{CSA,NC'}$ values measured for residue A26 were not included in calculating R_P nor in the subsequent CSA fitting procedure. We attribute this outlier to the nearly identical chemical shifts of T25 $^{13}C^{\alpha}$ and $^{13}C^{\beta}$ atoms (at 66.9 ppm), which result in incomplete decoupling of the ^{13}C aliphatic carbons during the constant-time ^{15}N evolution period to an extent that depends on the T25 ^{13}C′ spin state.

Relaxation of Backbone Amide ^{15}N−{^{2}H}. R_1 and $R_{1\rho}$ relaxation rates of the T11KK19EV42E mutant, dissolved in 100% D_2O, were measured at 600 MHz ^{1}H frequency and 283 K, using detection of $^{1}H^{\alpha}$ resonances in a modified H(CACO)N experiment (SI Figure S4). To identify residues that may be affected by conformational exchange contributions to the $R_{1\rho}$ rates, which are expected to be temperature dependent, $R_{1\rho}$ rates were also measured at 298 K. A comparison of these rates (Figure 3A) shows outliers for N8, T16, T17, N37, T53, and T54, identifying these residues as potentially having substantial R_{ex} contributions to their $R_{1\rho}$ rate at 283 K, but which due to the faster rates of these processes at 298 K become much smaller at the higher temperature. The estimated measurement error based on the scatter observed in Figure 3A (excluding the outliers) is 0.10 s^{-1}, or 3−5% of the observed rates. The slope of 1.38 ± 0.07 is consistent with the factor of 1.36 expected for the change in D_2O viscosity with temperature.

The ^{15}N−{^{2}H} R_1 rates of the same sample were also measured at 800 MHz and 283 K and correlate well with the 600 MHz data (Figure 3B). The scatter observed in that figure indicates a random measurement error of 0.018 s^{-1}, which corresponds to ca. 2%. We note that the correlation between R_1 rates measured at different fields is not expected to be completely linear for ^{15}N nuclei with different CSA tensors, with varying contributions from remote protons and a nonisotropic diffusion tensor, and therefore the scatter relative to a linear correlation provides an upper limit for the random error in R_1.

Due to the mass difference between ^{1}H and ^{2}H, the effective bond lengths of N−H and N−D are affected differently by their zero-point motions. The effect of zero point motions on the ^{15}N−^{1}H dipolar coupling, often expressed as a change in effective N−H bond length, previously has been studied by both quantum chemical calculations[66] and experimentally derived RDCs.[65] Here, we assume the equilibrium bond length of N-D, the length corresponding to the electron energy minimum, to be the same as that of the N−H bond since the electron energy is independent of the atomic mass. The amplitude of bond stretching motions is inversely proportional to the square root of the reduced mass of N−H or N-D, indicating a 27% reduction in the amplitude of N-D zero point bond stretching motions compared to N−H, reducing the increase in effective bond length, $r_{eff} = \langle r_{NH}^{-3}\rangle^{-1/3}$, from 0.007 for N−H to 0.005.

The change in effective dipolar coupling resulting from zero-point librational motion was estimated for the model compound NMA using normal-mode analysis, in the manner previously utilized by Case,[66] resulting in a 4.9% decrease in dipolar coupling, equivalent to a 0.017 Å increase in bond length, resulting in an effective N−D bond length of 1.030 Å, slightly shorter than the effective bond length of 1.040 Å for ^{15}N−^{1}H (Table 3). This 1.030 Å N−D bond length was used in all subsequent analyses. In principle, the substitution of ^{1}H by ^{2}H also perturbs the ^{15}N CSA value. However, as found by Tang and Case in their quantum computational analysis,[70] the ^{15}N CSA tensor orientation fluctuations are dominated by the adjacent heavier carbon atoms and not by motions of the amide proton or deuterium relative to the peptide bond, suggesting that the effect of zero-point motions on the CSA tensor is comparable for ^{15}N−^{2}H and ^{15}N−^{1}H sites. Therefore, this difference has been ignored in the fitting of the ^{15}N−^{2}H relaxation data.

Extracting Residue-Specific ^{15}N CSA Tensors. In our analysis, we simultaneously fit the ^{15}N RCSAs under six different alignment orientations, the ^{15}N CSA/N−H and ^{15}N CSA/N−C′ cross-correlated transverse relaxation rates, and the R_1 rates of the ^{15}N−^{2}H groups at two magnetic fields, 14.1 and 18.8 T. Under the common assumption that the ^{15}N CSA tensor is symmetric with respect to the peptide plane,[40] one of its principal components must be oriented orthogonal to this plane, and the orientation of the tensor is then defined by a single angle, β, between the N−H bond and its nearest in-plane principal component, which corresponds to the least shielded component, σ_{ZZ}, of the tensor (SI, Scheme S1). With the restriction that σ_{XX}

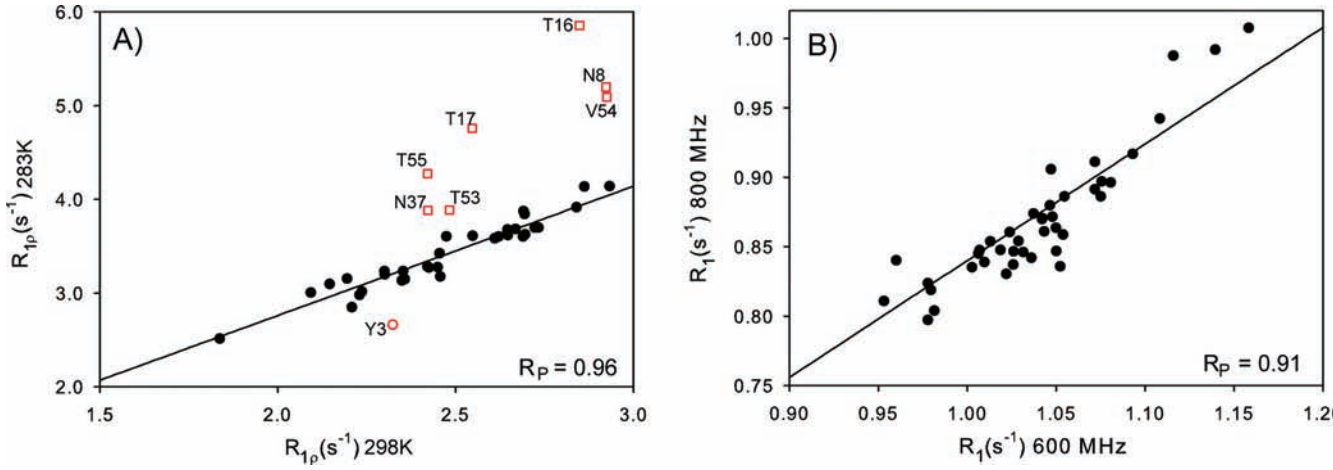

Figure 3. Correlation between relaxation rates measured for $^{15}N-\{^2H\}$ groups. (A) ^{15}N $R_{1\rho}$ rates, measured at 600 MHz ^1H frequency, for T11KK19EV42E in 100% D_2O at 283 and 298 K, both at 600 MHz ^1H frequency. Values from residues affected by conformational exchange are plotted as red squares; the rate measured for Y3 at 283 K was affected by overlap of its $^1H^\alpha$ chemical shift with the residual water signal. The solid line is the best linear fit and has a slope of 1.38. (B) ^{15}N R_1 rates of the same sample at 283 K, measured at magnetic fields corresponding to 600 and 800 MHz ^1H frequencies. The solid line corresponds to the theoretical ratio of 0.84 for a tumbling time of 6.6 ns.

Table 3. Effective N−H and N−D Bond Lengths of Backbone Amide Groups

	r_{eq}[a] (Å)	Δr_{str}[b] (Å)	Δr_{lib}[c] (Å)	r_{eff}[d] (Å)
N−H	1.008 ± 0.006	0.007[e]	0.025[e]	1.040[e] ± 0.006
N−D	1.008 ± 0.006	0.005	0.017	1.030 ± 0.006

[a] Equilibrium bond length determined from RDCs.[65] [b] Effective bond length increase due to zero point bond stretching motion, obtained from B3LYP/6-31G** QM calculations on N-methylacetamide in a water continuum solvent. [c] Effective bond length increase due to zero point bond librational motion, obtained from normal-mode analysis. [d] Effective bond length defined as $r_{eff} = r_{eq} + \Delta r_{str} + \Delta r_{lib}$. [e] From ref 66.

$+ \sigma_{YY} + \sigma_{ZZ} = 0$, two parameters suffice to define its principal components, and a total of three parameters therefore suffice to fully define the tensor. In the fit of the experimental data, two global parameters are optimized as well: the tumbling time of $^{15}N-^2H$ groups and a uniform generalized order parameter, S^2, describing all internal motions other than the zero-point librations and vibrations.

The backbone dynamics of GB3 and its nearly identical homologue GB1 previously has been studied extensively by both relaxation[44,73,82] and RDC-based methods.[64,65,84−89] Overall, the protein is found to be relatively rigid with the exception of a number of residues located in turn and loop regions, connecting elements of secondary structure. After excluding the residues found to have the lowest order parameters in the earlier relaxation study by Hall and Fushman,[73] including Q2, K10-E15, A20, D40-G41 and A48, a uniform order parameter, $S^2 = 0.903$, provided a best fit to all experimental data, well within their respective measurement errors. Although use of residue-specific S^2 values in the fitting procedure slightly lowers the χ^2 of the fit, introduction of such additional adjustable parameters proved unwarranted on the basis of F statistics, and also resulted in a slightly larger spread of the extracted CSA parameters and worse cross validation statistics. Use of a uniform order parameter in our analysis is conceptually equivalent to the assumption of uniform backbone dynamics by Wylie et al.[43] when deriving CSA values from the spinning sideband analysis observed for polycrystalline protein under slow magic angle spinning conditions.

In principle, the spectral density terms resulting from internal backbone dynamics also contributes to the relaxation rates, in particular to R_1. However, as reported by Hall and Fushman,[73] the longest internal correlation time τ_e in the well-structured region of the protein used for our analysis is 56 ps. For an average S^2 value of 0.903, this corresponds to an R_1 contribution less than 1.2% compared to that from overall tumbling.[90] For R_1 relaxation of $^{15}N-\{^2H\}$ nuclei in the protein dissolved in D_2O at 10 °C (τ_c = 6.6 ns), the fractional contribution from internal dynamics becomes even smaller (<0.6%) due to the relatively large R_1 contribution resulting from the overall tumbling $6J(\omega_N + \omega_D)$ term (taking into account the opposite signs of ω_N and ω_D). These contributions are smaller than the experimental measurement error, and therefore have been neglected.

Overall, for N residues, our fitting procedure then uses $3N + 2$ adjustable parameters, with nearly $10N$ experimental observables (a few residues lack one or two observables due to resonance overlap). Details of the data fitting procedure are presented in the Supporting Information.

Residue-specific ^{15}N CSA parameters are shown in Figure 4 (Table S3). The shielding anisotropy, $\Delta\sigma$ defined as $\sigma_{ZZ} - (\sigma_{XX} + \sigma_{YY})/2$,[91] shows an average value of −166 ppm with a standard deviation of 9 ppm over all residues included in the analysis. This average is very close to the value of −165 ± 7 ppm, determined by slow magic angle spinning solid state NMR for the closely homologous protein GB1[43] (averaged over the 33 amides for which values are obtained in both studies). With a correlation coefficient, $R_P = 0.8$, the $\Delta\sigma$ values extracted from

(84) Bouvignies, G.; Bernado, P.; Meier, S.; Cho, K.; Grzesiek, S.; Bruschweiler, R.; Blackledge, M. *Proc. Natl. Acad. Sci. U. S. A.* **2005**, *102*, 13885–13890.
(85) Markwick, P. R. L.; Bouvignies, G.; Blackledge, M. *J. Am. Chem. Soc.* **2007**, *129*, 4724–4730.
(86) Bouvignies, G.; Markwick, P. R. L.; Blackledge, M. *ChemPhysChem* **2007**, *8*, 1901–1909.
(87) Bouvignies, G.; Markwick, P.; Brueschweiler, R.; Blackledge, M. *J. Am. Chem. Soc.* **2006**, *128*, 15100–15101.
(88) Vogeli, B.; Yao, L.; Bax, A. *J. Biomol. NMR* **2008**, *41*, 17–28.
(89) Vogeli, B.; Ying, J. F.; Grishaev, A.; Bax, A. *J. Am. Chem. Soc.* **2007**, *129*, 9377–9385.
(90) Lipari, G.; Szabo, A. *J. Am. Chem. Soc.* **1982**, *104*, 4546–4559.
(91) Harris, R. K.; Becker, E. D.; De Menezes, S. M. C.; Granger, P.; Hoffman, R. E.; Zilm, K. W. *Pure Appl. Chem.* **2008**, *80*, 59–84.

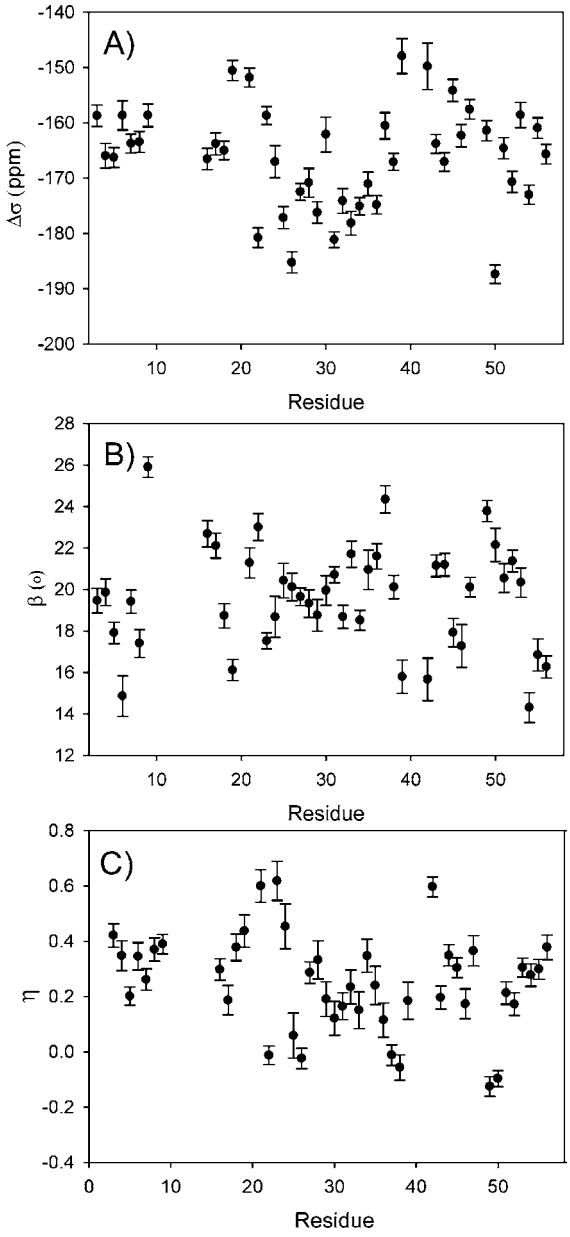

Figure 4. Residue specific ^{15}N CSA parameters derived from RCSA and relaxation data: (A) $\Delta\sigma = \sigma_{ZZ} - (\sigma_{XX} + \sigma_{YY})/2$; (B) the angle β between σ_{ZZ} and the N−H bond vector, while σ_{XX} and σ_{ZZ} are forced to fall in the C′−N−H^N plane; (C) the CSA asymmetry, η, defined as $(\sigma_{YY} - \sigma_{XX})/\sigma_{ZZ}$. Error bars correspond to the results of 100 Monte Carlo calculations, where Gaussian noise with an amplitude corresponding to the estimated root-mean-square error was added to the experimental input data.

our data correlate fairly well with these values too (SI, Figure S8), but less well with values derived by the same group using the ROCSA method ($R_P = 0.5$), which also are systematically smaller.[42] We note, however, that neither set of solid-state NMR values accounts for the effect of backbone internal dynamics. Assuming that the amplitude of such dynamics is comparable in solution and in the solid state, our solution values which correspond to the absence of thermal motions, need to be scaled by the average order parameter, $S = \sqrt{0.903}$, prior to comparison to the solid state NMR data and the average $\Delta\sigma$ (158 ppm) then falls in between the ROCSA and slow MAS results.

The average CSA value obtained from our study falls close to the value of -164 ± 19 obtained by Hall and Fushman from auto- and cross-relaxation rates measured for the same protein at five magnetic field strengths (this average extends over the same group of residues evaluated in our study and has been scaled by 1.06 to eliminate the zero-point librational contribution). Site-to-site variations are considerably smaller in our study, suggesting that RCSA and R_1 rates of ^{15}N−{^{2}H} provide useful independent additional constraints for CSA fitting, thereby reducing the effect of random and systematic measurement errors.

Our solution NMR measurements also yield the orientation of the ^{15}N CSA tensor relative to the peptide group. With $\beta = 19.6 \pm 2.5°$, we find tight clustering of the orientations of the least shielded σ_{ZZ} axis relative to the N−H bond. However, considerable variation in the shielding asymmetry parameter η, defined as $(\sigma_{YY} - \sigma_{XX})/\sigma_{ZZ}$,[91] is observed: $\eta = 0.23 \pm 0.17$ for α-helix, and $\eta = 0.31 \pm 0.11$ for β-sheet. Interestingly, for six residues (five of them outside regions of regular secondary structure, SI Table S3) we find that the most shielded CSA component is orthogonal to the peptide plane, and following IUPAC nomenclature the *X* and *Y* axis of the CSA tensor would need to be interchanged.[91] However, in order to facilitate comparison of the different amide CSA tensors, we retain the same orientation, resulting in negative η values for these residues.

Significant correlations between the CSA parameters and the type of secondary structure are observed in our study. For β-strand residues, we find $\langle\Delta\sigma\rangle = -162 \pm 6$ ppm, whereas considerably larger CSA is observed for α-helical amide groups: $\langle\Delta\sigma\rangle = -173 \pm 7$ ppm. Statistically significant differences between CSA parameters in β-strand and α-helical residues pertain to all three components (Table 4). By including the variation in isotropic chemical shift, we can now evaluate which components of the shift tensor are affected most by secondary structure. Using $\delta_{ii} = \delta_{\text{isotropic}} - \sigma_{ii}$, yields average values of $\delta_{ZZ} = 230 \pm 7$, $\delta_{XX} = 52 \pm 8$, and $\delta_{YY} = 85 \pm 9$ ppm for β-sheet and 236 ± 6, 49 ± 8, and 76 ± 10 ppm for the α-helix, indicating that the ^{15}N nucleus in β-strand, on average, is more shielded in the *Z* direction, and less shielded in *X* (3 ppm) and *Y* directions (9 ppm) (scheme S1). These data indicate that the, on average, downfield isotropic ^{15}N shift in β-sheet relative to α-helix results from decreased shielding in the X and Y directions, which outweigh an actual increase in shielding in the *Z* direction.

Previously, a correlation between δ_{ii} values and isotropic chemical shifts was noted for backbone amides in ubiquitin.[40] Somewhat stronger correlations are found in our present study of GB3 (Figure 5) where, for example, the correlation coefficient R_P between δ_{ZZ} and $\delta_{\text{isotropic}}$ equals 0.73, versus 0.41 for ubiquitin.

Validation of CSA Parameters. To validate the quality of the residue-specific CSA values, derived in our study, the R_2 rates of ^{15}N−{^{2}H} backbone amides, which are dominated by CSA relaxation, were calculated on the basis of the above derived CSA tensors and compared to the experimental values. Note that these experimental ^{15}N−{^{2}H} R_2 rates were not included at any stage in deriving the CSA values. A strong correlation ($R_P = 0.94$) between observed and predicted rates is obtained, compared with $R_P = 0.53$ when a uniform CSA (average of the residue-specific CSA values) tensor is used (Figure 6). For an isolated ^{15}N−{^{2}H} two-spin system subject to isotropic tumbling, the predicted R_2 rates are uniform when a uniform CSA tensor is utilized. The small variation in predicted R_2 rates, even for a uniform CSA tensor (Figure 6B) results from anisotropic molecular tumbling, and also from small contributions from

Table 4. Fitted CSA Tensors for α Helix, β Strand, and Overall Protein

	σ_{ZZ} (ppm)	σ_{XX} (ppm)	σ_{YY} (ppm)	β (°)	$\Delta\sigma$ (ppm)	η
α helix[a]	−115 ± 5	71 ± 8	44 ± 11	19.8 ± 1.2	−173 ± 7	0.23 ± 0.17
β strand [a]	−108 ± 4	71 ± 4	38 ± 7	18.8 ± 2.4	−162 ± 6	0.31 ± 0.11
all[a]	−111 ± 8	69 ± 11	42 ± 9	19.6 ± 2.5	−166 ± 9	0.25 ± 0.17

[a] Average and standard deviation for CSA tensor components experimentally derived for the backbone amide ^{15}N nuclei in GB3. Values apply to the absence of thermal motions, i.e., $\Delta\sigma$ values observed by solid state NMR are expected to be scaled down by $\sqrt{(S^2)} \approx 0.95$ relative to values reported in the table. Three parameters ($\Delta\sigma$, η, β) are fitted for each ^{15}N site. The root-mean-square deviations from the reported averaged values reflect the CSA variability in α helix, β strand, and all residues.

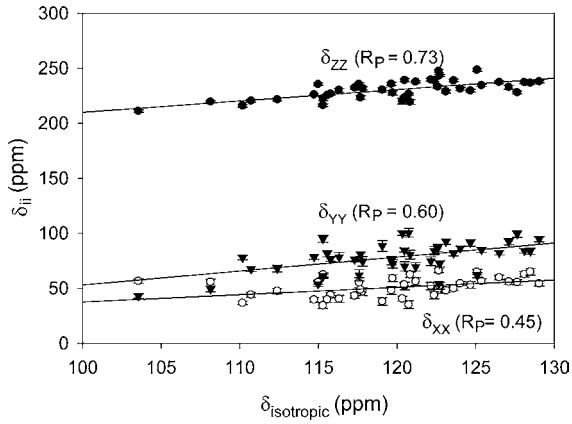

Figure 5. Correlation between the principal components of the chemical shift tensor δ_{ii} ($i = X, Y, Z$) and the isotropic chemical shift $\delta_{\text{isotropic}}$. The three best fitted lines correspond to $\delta_{ZZ} = 1.03\delta_{\text{isotropic}} + 107$ ppm, $\delta_{YY} = 1.33\delta_{\text{isotropic}} - 82$ ppm, and $\delta_{XX} = 0.63\delta_{\text{isotropic}} - 25$ ppm.

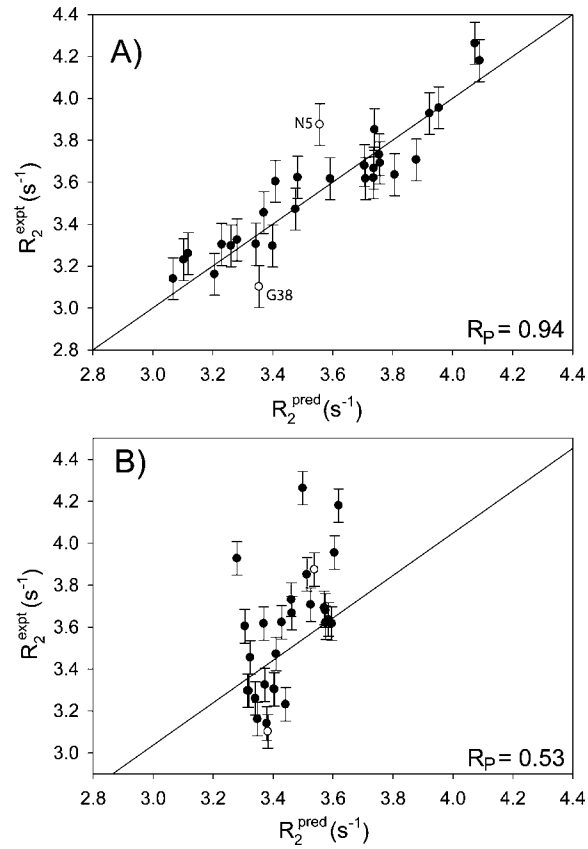

Figure 6. Correlation between experimental and predicted R_2 rates of ^{15}N−{^{2}H} groups. Predicted rates were calculated from (A) experimental site-specific ^{15}N CSA values or (B) from using a uniform, averaged CSA tensor. The solid line in panel A represents the best linear fit with zero intercept and has a slope of 1.00 (excluding two outliers, N5 and G38).

passive ^{1}H and ^{13}C nuclei. The correlation coefficient of 0.94 is also higher than the corresponding value of 0.84 obtained when correlating the experimental and predicted R_2 rates using the solid state CSA values of the homologous GB1 protein (SI, Figure S9A). These latter data lack information on the orientation of the CSA tensor within the peptidyl frame, and therefore a uniform value $\beta = 19.6°$ was assumed.

Considering that the root-mean-square variation in β angle in our residue-specific CSA values is only 2.5°, it is interesting to explore the impact of fixing this parameter rather than letting it vary on a residue-by-residue basis. Therefore, we also carried out a fit of all experimental data (excepting again the ^{15}N−^{2}H R_2 data) while fixing β at 19.6°, while allowing $\Delta\sigma$ and η to vary residue by residue. When using the CSA parameters resulting from this approach to predicted the ^{15}N−^{2}H R_2 rates, a somewhat lower correlation with the experimental rates is observed ($R_P = 0.90$; SI, Figure S9B). Even though the R_2 value to first order is not sensitive to the orientation of the CSA tensor, restricting β during the fitting procedure results in small changes of the best fitted principal components of the CSA tensors. The lower agreement between experimental and predicted R_2 values obtained with a fixed β angle confirms that the small β variations obtained when letting this parameter float do not result from random measurement error.

For the vast majority of residues, the most shielded CSA tensor component is located in the peptide plane, nearly parallel to the N−C′ bond, but the difference in magnitude relative to the component orthogonal to the peptide plane is modest. To assess the significance of permitting asymmetry as a variable parameter in the fit, we also carried out the entire CSA fitting procedure while fixing the tensor to be axially symmetric, i.e. $\eta = 0$, and use the resulting CSA tensors again to predict the R_2 values. Pearson's correlation coefficient R_P between the experimental and predicted R_2 values then drops to 0.86 (SI, Figure S9C), again significantly lower than the $R_P = 0.94$ value obtained when η is a fitted parameter. The effect of asymmetry of the CSA tensor on relaxation rates scales with $(1 + \eta^2/3)$, and in this case the lower correlation appears to be dominated by the neglect of the $\eta^2/3$ component, rather than the small changes in $\Delta\sigma$ caused by the $\eta = 0$ restriction during the fit.

Orientation of ^{15}N CSA Tensor. Above, the principal axes of σ_{XX} and σ_{YY} were restrained in our fitting such that one component is orthogonal to the peptide plane. Removal of this restriction increases the number of adjustable parameters to five, but more importantly it makes it difficult to establish the precise orientations of the σ_{XX} and σ_{YY} axes when the difference between σ_{XX} and σ_{YY} is small, as applies for many of the backbone amide ^{15}N nuclei in GB3. Therefore, in order to validate the assumption that the CSA tensor is symmetric with respect to the peptide plane, we forced the CSA tensor values and orientations relative to their respective peptide plane to be uniform within each type of secondary structure. This latter clause reduces the ratio of

the number of fitted parameters over the number of experimental observables and thereby increases the robustness of the analysis.

Three angles, together with $\Delta\sigma$ and η, are fitted simultaneously for all helical residues, and similarly for all β-strand residues. For the fit, the generalized order parameter S^2 is fixed at the above derived value of 0.903, and the tumbling time for the protein in D_2O (required for analysis of the $^{15}N-\{^2H\}$ R_1 data) is fixed at the above derived value of 6.63 ns. The principal components and orientations obtained when following this procedure (SI, Table S6) confirm that the CSA amplitudes and β angles are consistent with the averages obtained from their respective site specific values (Table 4). The fitting procedure also confirms that the orientation of σ_{YY} remains nearly perpendicular to the peptide plane, deviating from orthogonality by 2.5° and 0.6° for α helix and β strand, respectively, while σ_{XX} essentially remains in the peptide plane. This result supports the validity of the assumption made in our site-specific ^{15}N CSA analysis that the CSA tensor to a very good approximation is symmetric with respect to the peptide plane, despite the chiral nature of the adjacent C^α carbons. Note, however, that the average orientation of the *Y* axis of the CSA tensor, determined for each type of secondary structure, is dominated by residues with the largest η value, for which the χ^2 is far more sensitive to this orientation than for small η values, with the definition of its orientation in the *XY* plane becoming arbitrary for $\eta = 0$. Larger deviations from orthogonality to the peptide plane for small η values are therefore not excluded by our data.

Origin of ^{15}N CSA Variations. The ca. 10 ppm larger ^{15}N CSA observed in α helix compared to β strand (Table 4) confirms the effect of the backbone torsion angles on the CSA tensor, and agrees closely with the 9 ppm difference found by slow-spinning solid state NMR.[92] This value is opposite in sign and much smaller than the average −24 ppm difference obtained from vacuum calculations on partially geometry-optimized peptide fragments[19] but close to the +4 ppm difference obtained from lower basis set calculations on hydrated dipeptide models by Cai et al.[20] In order to further evaluate the factors underlying the differences in CSA, which are known to be impacted by a wide variety of factors, we carried out additional DFT calculations for closely related fragments at a high level of theory. Even though the effect of hydration then cannot easily be included, these calculations are aimed to evaluate the trends behind the experimentally observed differences in CSA.

Our DFT calculations on formyl-$(Ala)_2$ yields chemical shift tensor components (δ_{XX}, δ_{YY}, and δ_{ZZ}) of 219, 30, and 97 ppm for the helical conformation (using Ψ and ϕ torsion angles of T25 and A26) and 218, 36, and 98 ppm for a β-strand (Ψ and ϕ angles of F52-T53 in GB3) conformation (Table S7). Even though the calculated values deviate substantially from the experimental ones, likely caused by the simplicity of the model, the difference between α-helix and β-strand geometries points in the same direction as the experimental results.

Two GB3 residues, V21 and A23, show exceptionally high η values, 0.62 and 0.60, respectively (Table S3). Interestingly, DFT calculations on formyl-$(Ala)_2$ with ϕ and Ψ angles of A20-V21 and D22-A23 also yield larger η values, 0.84 and 0.86, than computed for α-helical (0.64) and β-strand (0.61) conformations. The (ϕ, Ψ) angles are (−154°, 159°) for A20, (−77°,−24°) for V21, (−152°, 168°) for D22, and (−67°, −36°) for A23, suggesting that an extended followed by an α-helical conformation peptide linkage tends to result in larger η values. Exceptionally low experimental η values are found for G38 (−0.06) and K50 (−0.10). DFT calculations on formyl-$(Ala)_2$ with the backbone torsion angles of T49-K50 and formyl-Ala-Gly with the N37-G38 backbone torsion angles yield η values of 0.23 and 0.28, suggesting that (ϕ, Ψ) combinations of (−112°, 3°) and (51°, 43°) for T49-K50 and similarly (−101°, 10°) and (72°, 21°) for N37-G38 generate small η values. It is worth noting that the DFT calculations in this study are oversimplified as other effects such as side chain types and torsion angles, long-range electrostatics, solvent interaction, etc., are ignored. Instead of attempting to reproduce the experimental CSA values, these calculations aim to simply explore the importance of the backbone (ϕ, Ψ) angles. The close correspondence between trends seen in calculated CSA values and experimentally observed values points to a dominant effect from the backbone torsion angles on the CSA magnitude and asymmetry (SI Table S7).

Discussion

The value of the ^{15}N backbone amide chemical shift anisotropy tensor affects both solid state NMR structural studies, in particular those based on analysis of ^{15}N chemical shifts in oriented membrane proteins as studied by PISEMA analysis, as well as the quantitative evaluation of protein dynamics from ^{15}N relaxation rates measured by solution NMR. The precise eigenvalues and orientation of the ^{15}N CSA also affect the degree of cancellation between dipolar and CSA interactions which underlies the important TROSY experiment,[25] and determines the field strength at which the minimum ^{15}N TROSY line width is reached, as well as the maximum degree of cancellation of dipolar and CSA contributions possible for an isolated $^{15}N-^1H$ spin pair. Below, we briefly discuss the impact of ^{15}N CSA variations on these latter two areas.

Impact on ^{15}N Relaxation Studies. Most prior analyses of protein backbone dynamics from ^{15}N relaxation data assume an axially symmetric ^{15}N CSA tensor with a $\Delta\sigma$ value of either −160 or −170 ppm. A second important parameter includes the length of the N−H bond vector, often assumed to be 1.02 Å. However, when factoring out the nearly uniform attenuation of the $^{15}N-^1H$ dipolar coupling caused by zero-point librations of the N−H bond, this becomes equivalent to using a 1.04 Å effective N−H bond length,[66,93] accompanied by a concomitant increase in the order parameters, S^2, extracted from NMR relaxation rates.

When using a 1.04-Å effective N−H bond length, our data correspond to an average ^{15}N $\Delta\sigma$ value of −166 ppm, which represents the effective CSA averaged over the zero-point backbone motions, i.e., the CSA that would be measured at 0 K, in the absence of thermally activated motions. Considering that the difference between α-helical and β-sheet residues is quite pronounced, approximately two standard deviations, a better choice in ^{15}N relaxation analysis is the use of secondary structure-specific CSA tensors, with $\Delta\sigma = -162$ ppm and $\eta = 0.31$ for β-sheet residues, and $\Delta\sigma = -173$ ppm, $\eta = 0.23$ for helical residues. If instead the nonlibrationally corrected N−H bond length of 1.015 Å were used, this should be accompanied by an average $\Delta\sigma$ value of −179 ppm, and will then result in a uniform 7% reduction in derived order parameters (13.5% for S^2). It is important to note that this −179 ppm CSA value does not correspond to the CSA of the protein at 0 K and has no direct physical meaning; instead it is an artificial number

(92) Wylie, B. J.; Rienstra, C. M. *J. Chem. Phys.* **2008**, 128.

(93) Ottiger, M.; Bax, A. *J. Am. Chem. Soc.* **1998**, *120*, 12334–12341.

used to match the CSA order parameter with the dipole−dipole order parameter if one were to use a nonlibrationally corrected $r_{NH} = 1.015$ Å value.

Prior analyses of NMR relaxation data and their field dependence alternately have been interpreted as indicative of rather large residue-by-residue variations in the ^{15}N CSA tensor,[33,44] or as evidence for much higher CSA uniformity.[35,39] Much of the difference in the conclusions from the very similar experimental data appears to relate to the magnitude of the experimental errors assumed in the relaxation measurements, with larger experimental errors requiring less variation in the CSA parameters to fit the experimental data. Although the random measurement error is easily estimated from reproducibility of experimental results, quantitative estimates of systematic errors are difficult to make as their origins in many cases are unknown, and neither conclusion appears definitive in the absence of such information.

Cross-correlated relaxation measurements yield additional information on the orientation of the CSA tensor. Provided that relaxation interference between the CSA and multiple dipolar interactions can be measured separately, such measurements also can yield the deviation from axial symmetry of the ^{15}N CSA tensor. Measurements for ubiquitin by Loth et al, for example, show a correlation between the tensor asymmetry, η, and the isotropic ^{15}N chemical shift.[40] On the other hand, two separate sets of solid state NMR measurements of the ^{15}N CSA tensors in polycrystalline GB1, one using the recoupling of chemical shift anisotropy or ROCSA method,[42,94] and a more recent one that uses slow magic angle spinning sideband analysis,[43] do not show any such correlation between η and δ_{iso} (Figure S1). Although these latter two sets of measurements correlate fairly well with one another ($R_P = 0.77$), the ROCSA method $\Delta\sigma$ values are systematically smaller than the more recent values by nearly 10%, and therefore do not quite answer the question about how large the ^{15}N CSA truly is. Our current measurements on GB3 agree most closely with the slow magic angle spinning results on the homologous GB1 protein, and also lack any significant correlation between η and δ_{iso}. Instead, it appears η is dominated by backbone torsion angles. In particular, the only non-Gly residue with positive values for its ϕ backbone torsion angle shows an inverted sign for η, when keeping σ_{YY} oriented orthogonal to the peptide plane. Similarly, the measurements by Loth et al. also yield η values much below average for all three non-Gly residues in ubiquitin with positive ϕ angles.

The effect of asymmetry of the CSA tensor on the R_1 and R_2 relaxation rates scales with $(1 + \eta^2/3)$, equivalent to scaling the magnitude of the CSA by $(1 + \eta^2/3)^{1/2}$. For most residues, $\eta \leq 0.4$, and the asymmetry increases the effective magnitude of the CSA by less than 2.6%, or ~4 ppm. However, for some residues, such as V21 and A23 in GB3, $\eta > 0.6$ and the tensor asymmetry increases the effective magnitude by as much as 10 ppm.

As was the case for the prior solid-state NMR studies of ^{15}N CSA in polycrystalline proteins, our analysis assumes that the observed RCSA values are scaled uniformly by a generalized order parameter, S, which has a uniform value ($\sqrt{0.903}$) for all residues considered. Residues that clearly exhibit elevated internal dynamics based on prior relaxation measurements therefore were excluded from our analysis. As expected, if in addition to the CSA tensor, S^2 is treated as a residue-specific adjustable parameter, a better fit to the NMR data is obtained. However, the nearly 30% improvement in terms of χ^2 statistics is insufficient to warrant inclusion of these extra variables in the fitting procedure (F value equals 2.57, smaller than the critical value of $F_{(1,6,0.05)} = 5.99$).[95] Notably, the spread in the extracted CSA values increases from ± 9 to ± 16 ppm, and for most residues then correlates inversely with the value of S (data not shown). Because such an inverse correlation clearly points to overfitting of the experimental data, use of a residue-specific S^2 value is not warranted for the well-ordered regions of GB3. However, true variations in S^2 will contribute to the variability of the observed CSA magnitude, and the variability in $\Delta\sigma$ extracted from our data, as well as that seen in the solid state NMR results, therefore provides an upper limit for the true variability.

It previously has been shown from both NMR relaxation measurements and molecular dynamcis simulations[96] as well as RDC measurements.[61,64,84] that motions of the N−H vector are axially asymmetric, with largest amplitudes around the $C^\alpha-C^\alpha$ axis (so-called γ motions in the Gaussian axial fluctuation or GAF model). In contrast to isotropic motion, anisotropic motion scales the CSA components σ_{XX}, σ_{YY}, and σ_{ZZ} differentially. However, in practice, it is very difficult to separate isotropic from anisotropic motions for two reasons: First, zero-point librations, though anisotropic, scale σ_{XX}, σ_{YY}, and σ_{ZZ} more uniformly than thermal motions,[70] but separating anisotropic zero point motion from thermally activated motions is experimentally difficult. Second, while in the fitting of the relaxation and RCSA data, the anisotropic internal motion effectively makes the dipole−dipole interaction tensor asymmetric, whereas the contribution to the CSA tensor is virtually indistinguishable from a change in asymmetry (and magnitude) of the already asymmetric CSA tensor. When imposing uniform motional asymmetry of all peptide plane motions using the GAF model[84,96] while restraining the total order parameter S^2 at 0.903, essentially no change of the total fitting error is obtained, even though the magnitudes of σ_{ZZ} and σ_{YY} increase slightly with increasing amplitudes of the γ motions around the $C^\alpha-C^\alpha$ axis (and decreasing amplitudes of motions orthogonal to this axis to keep $S^2 = 0.903$; data not shown).

It also is worth pointing out that random experimental errors in any of our measurements will generally increase the spread in the extracted CSA values. Therefore, even disregarding the effect of variations in S^2, the true spread in CSA values is expected to be somewhat smaller than the standard deviation of ±9 ppm reflected in the values shown in Figure 4A (±6−7 ppm within sheet or helix).

As highlighted by Damberg et al.,[39] the modelfree generalized order parameters extracted from NMR relaxation measurements vary with the value of the assumed $\Delta\sigma$ parameter, and in particular at high magnetic field strengths (e.g., 800 or 900 MHz ^1H frequency) extracted S^2 values are quite sensitive to $\Delta\sigma$.

To explore the impact of our experimental CSA variation on S^2, we performed the standard model-free analysis[90,97] using our site-specific ^{15}N CSA values to fit experimental $R_1(^{15}N-^1H)$ and $R_2(^{15}N-^1H)$ values and the NOE data from Hall and Fushman[83] with two parameters, the local internal motion time constant, τ_e and S^2. The values obtained for the 30 residues

(94) Chan, J. C. C.; Tycko, R. *J. Chem. Phys.* **2003**, *118*, 8378–8389.
(95) Bevington, P. R.; Robinson, D. K. *Data reduction and error analysis for the physical sciences*; McGraw-Hill: New York, 1992.
(96) Lienin, S. F.; Bremi, T.; Brutscher, B.; Bruschweiler, R.; Ernst, R. R. *J. Am. Chem. Soc.* **1998**, *120*, 9870–9879.
(97) Mandel, A. M.; Mikael, A.; Palmer, A. G. *J. Mol. Biol.* **1995**, *246*, 144–163.

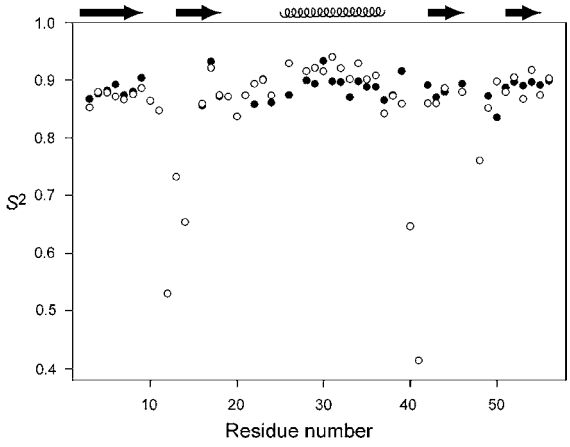

Figure 7. Order parameters, S^2, from model-free analysis using uniform CSA (open circles) and site-specific CSA (filled circles) values. Site specific CSA values are only available for residues previously identified as rigid (see text). For the sake of completeness, the results obtained for the more flexible residues (using uniform CSA) are also shown.

located in GB3′s β-sheet and α-helix, determined using site-specific ^{15}N CSA values, are highly homogeneous, yielding $S^2 = 0.888 \pm 0.017$. For the purpose of comparison, when performing the same model-free analysis on the same set of amides, but using a uniform, averaged ^{15}N CSA tensor, considerably more variation is seen: $S^2 = 0.892 \pm 0.025$ (Figure 7). The nearly 50% increase in S^2 variation when using uniform instead of site-specific ^{15}N CSA strongly suggests that variations in the extracted S^2 values among the well structured residues are significantly affected by variations in CSA. We note that the remaining small spread of ±0.017 in S^2 includes contributions from random measurement errors in the ^{15}N R_1 and R_2 rates, as well as from residual uncertainty in the CSA values extracted in our present study. For example, the rmsd value when using site-specific CSA values is dominated by the high order parameter obtained for F30, for which a far below average value of $\Delta\sigma$ is obtained. However, we note that for this residue no ^{15}N−{^{2}H} R_1 input data were available, and its CSA value is therefore less well determined than for most other residues. The S^2 spread of ±0.017 therefore represents an upper estimate for the true variation in backbone order, indicating that dynamic backbone behavior on the fast time scale in secondary structure regions of GB3, and presumably of many other proteins too, is considerably more homogeneous than indicated by previous NMR relaxation studies. At the same time, the small degree of variation observed for S^2 (1.9%, or 1% for S) confirms that the assumption of a uniform S value is not unreasonable, and that the derived ^{15}N CSA variation 5.4% is dominated by true site-to-site differences, and not by variations in dynamics.

Impact on ^{15}N TROSY Spectra. Most predictions of ^{15}N resolution enhancement attainable with transverse relaxation optimized spectroscopy (TROSY)[25] are based on the assumption of a uniform, axially symmetric ^{15}N CSA tensor. Variations in the magnitude, asymmetry, and orientation of the ^{15}N CSA tensor will impact the TROSY ^{15}N line width, however, as well as the optimal field strength where the line width is narrowest. Indeed, considerable variation in the TROSY line widths, calculated when using the CSA values derived for GB3, manifests itself in a standard deviation that represents a significant fraction of the line width (Figure 8A). To eliminate small contributions from diffusion anisotropy or variations in order parameter, values are calculated under the assumption of isotropic diffusion with a tumbling time of 50 ns and a uniform

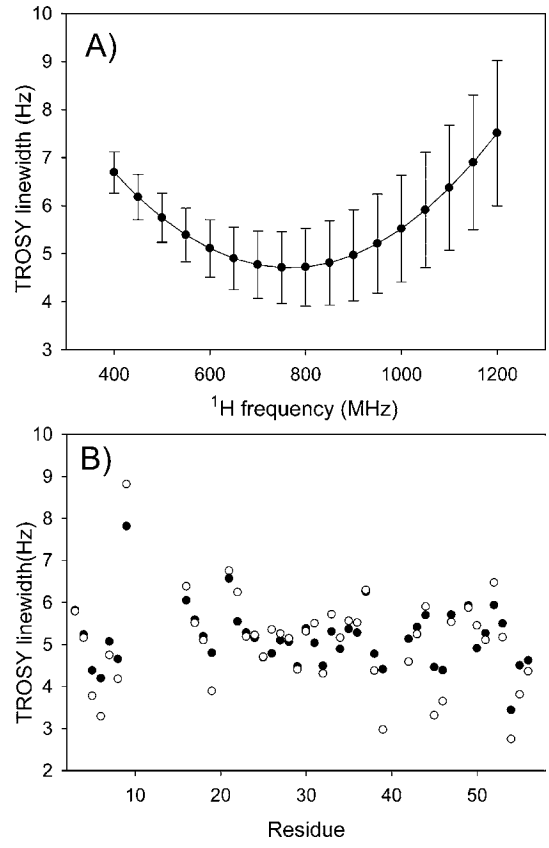

Figure 8. Calculated TROSY line widths for ^{15}N nuclei in GB3, assuming isotropic rotational diffusion with a correlation time of 50 ns, and idealized two-spin approximations for each amide group (i.e., ignoring the presence of other spins and relaxation mechanisms other than ^{15}N CSA and ^{15}N−^{1}H dipolar), using experimentally derived CSA tensors and uniform $S^2 = 0.903$ values. (A) Average TROSY line widths and standard deviations as a function of field strength. (B) Residue specific ^{15}N TROSY line widths calculated for magnetic field strengths corresponding to ^{1}H frequencies of 600 MHz (filled symbols) and 900 MHz (open symbols).

$S^2 = 0.903$. On average, the minimum line width is obtained at ca. 800 MHz ^{1}H frequency, well below the value of ca. 1 GHz predicted when using earlier CSA parameter values,[25] and as anticipated the variation in intrinsic line width increases with field strength. For example the standard deviation of the calculated line widths increases from 0.6 Hz (or 12%) at 600 MHz to 0.95 Hz (19%) at 900 MHz. The residue-specific TROSY peak line widths calculated for field strengths corresponding to 600 and 900 MHz ^{1}H frequency show that for some residues the ^{15}N TROSY line width is narrower at 600 MHz (e.g., V54 and T55), whereas for others predicted line widths are narrowest at 900 MHz (Figure 8B). Note that these intrinsic line widths neglect mechanisms that add a nearly field-independent contribution from dipolar couplings to ^{13}C, ^{2}H, and residual remote ^{1}H nuclei, as well as the nonzero R_1 relaxation rate of $^1H^N$. As can be seen, the largest line width is predicted for the amide of G9 which is 53% (77%) larger than the average value at 600 (900) MHz ^{1}H frequency, while the smallest one is found for V54, which is 33% (55%) below the average value predicted at 600 (900) MHz. G9 has the largest β angle 25.9° and V54 has the smallest β angle 14.3° (Figure 4B), highlighting the fact that the cancellation of dipolar and CSA contributions, which underlies the TROSY experiment, is more affected by variations in the angle β than by differences in the magnitude or asymmetry of the CSA tensor. For example, if the β angle is set to 19.6°, but the site-specific CSA values are used to

calculate the TROSY line widths, the rms variation in line width drops from 0.6 to 0.41 Hz at 600 MHz or from 0.95 to 0.46 Hz at 900 MHz, and residues G9, and V54 are no longer outliers. The remaining line width variation then results from residue by residue variation in the CSA magnitude and asymmetry.

Acknowledgment. We thank Dennis A. Torchia and Jinfa Ying for helpful discussions and Werner Maas and Jochem Struppe (Bruker Instruments) for help with the MAS measurements. This work was supported in part by the Intramural Research Program of the NIDDK, NIH, by the Intramural AIDS-Targeted Antiviral Program of the Office of the Director, NIH, and by NIH grants P41RR02301 (BRTP/NCRR) and P41GM66326 (NIGMS) to G.C.

Supporting Information Available: A detailed description of the equations and protocols used for analysis of the relaxation and dipolar coupling data, three figures with pulse diagrams used for the measurement of cross-correlated relaxation and $^{15}N-\{^2H\}$ R_1 and R_2 relaxation rates; two figures comparing η and Δ with solid state values reported for GB1, 6 figures correlating the difference between observed and expected $\Delta\delta(^1H)$ with the ^1H temperature coefficients; one figure comparing observed with best-fitted R_2/R_1 ratios; one figure comparing $\Gamma^{CSA,NH}$ values measured with two different transverse evolution delays; 3 figures correlating $^{15}N-\{^2H\}$ R_2 experimental and predicted values; 2 figures showing experimental data used for deriving $\Gamma^{CSA,NH}$ and $\Gamma^{CSA,NC'}$ values; one table with apparent ^1H temperature coefficients; one table with the temperature differences for cryogenic and MAS probes; one table with experimentally derived $\Delta\sigma$, η, and β values; one table with experimental RCSA values; one table with experimental $^{15}N-\{^1H\}$ R_1, R_2, $\Gamma^{CSA,NH}$, and $\Gamma^{CSA,NC'}$ values; one table listing the CSA tensors. This material is available free of charge via the Internet at http://pubs.acs.org.

JA910186U